AD-A283 655

NAVAL POSTGRADUATE SCHOOL
Monterey, California

DTIC
SELECTED
AUG 2 4 1994
F
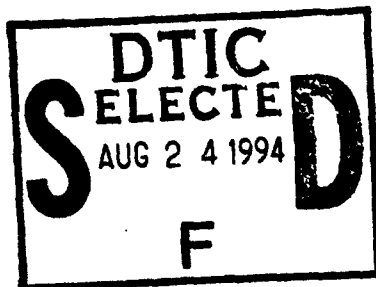
THESIS

94-26890

CALIBRATION AND SEDIMENT LOAD
ALGORITHMS FOR AN ACOUSTIC
SEDIMENT FLUX PROBE

by

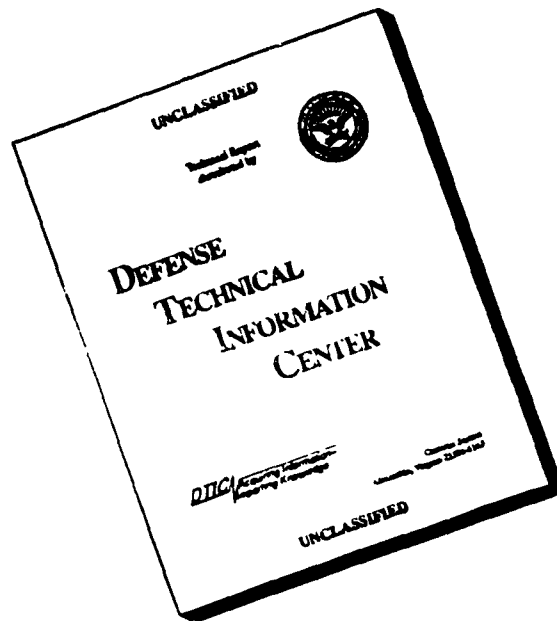Weston J. Anderson

June 1994

Thesis Advisor:	Timothy P. Stanton
Thesis Co-Advisor:	Edward B. Thornton

94 8 23 047

DISCLAIMER NOTICE

REPORT DOCUMENTATION PAGE

Form Approved OMB No. 0704

1. AGENCY USE ONLY *(Leave blank)*	2. REPORT DATE June 1994.	3. REPORT TYPE AND DATES COVERED Master's Thesis

4. TITLE AND SUBTITLE CALIBRATION AND SEDIMENT LOAD ALGORITHMS FOR AN ACOUSTIC SEDIMENT FLUX PROBE	5. FUNDING NUMBERS
6. AUTHOR(S) Weston J. Anderson	
7. PERFORMING ORGANIZATION NAME(S) AND ADDRESS(ES) Naval Postgraduate School Monterey CA 93943-5000	8. PERFORMING ORGANIZATION REPORT NUMBER
9. SPONSORING/MONITORING AGENCY NAME(S) AND ADDRESS(ES)	10. SPONSORING/MONITORING AGENCY REPORT NUMBER

11. SUPPLEMENTARY NOTES The views expressed in this thesis are those of the author and do not reflect the official policy or position of the Department of Defense or the U.S. Government.

12a. DISTRIBUTION/AVAILABILITY STATEMENT Approved for public release; distribution is unlimited.	12b. DISTRIBUTION CODE A

13. ABSTRACT *(maximum 200 words)*

A method to infer sediment concentrations from acoustic backscatter levels has been implemented for a prototype acoustic sediment flux probe. This required calibrations of the acoustic transceiver systems and direct measurements of the system response to typical sediment size distributions over a wide range of concentrations.

The sensitivities of the 1.3 MHz and 5.2 MHz transducers of an acoustic sediment probe were measured using the backscatter amplitudes from stainless steel wires of four different radii. A two-frequency inversion algorithm estimating the geometric mean radius and variance about the mean of suspended sediment with an assumed lognormal size distribution and the sediment mass concentration was developed and tested in a laboratory setting.

The sensitivity of the 5.2 MHz transducer for each wire was consistent within 10%. The sensitivity of the 1.3 MHz transducer calculated for each wire was not consistent and is believed to be due to a strong angular dependence between the wire orientation and the 1.3 MHz transducer face. The sensitivities of each of the four transducers were, however, inferred from the system's response to the controlled sediment backscatter measurements.

14. SUBJECT TERMS sediment flux, acoustic backscatter, acoustic sediment flux probe, transducer sensitivity	15. NUMBER OF PAGES 95
	16. PRICE CODE

17. SECURITY CLASSIFICATION OF REPORT Unclassified	18. SECURITY CLASSIFICATION OF THIS PAGE Unclassified	19. SECURITY CLASSIFICATION OF ABSTRACT Unclassified	20. LIMITATION OF ABSTRACT UL

i

Calibration and Sediment Load Algorithms
for an Acoustic Sediment Flux Probe

by

Weston J. Anderson
Lieutenant, ' ' d States Navy
B.S., University N Mexico, 1986

Submitted in partial fulfillment
of the requirements for the degree of

MASTER OF SCIENCE IN METEOROLOGY
AND PHYSICAL OCEANOGRAPHY

from the

NAVAL POSTGRADUATE SCHOOL
June 1994

Author: _____
Weston J. Anderson

Approved by: _____
Timothy P. Stanton, Thesis Advisor

_____
Edward B. Thornton, Second Reader

_____
Curtis A. Collins, Chairman
Department of Oceanography

ABSTRACT

A method to infer sediment concentrations from acoustic backscatter levels has been implemented for a prototype acoustic sediment flux probe. This required calibrations of the acoustic transceiver systems and direct measurements of the system response to typical sediment size distributions over a wide range of concentrations.

The sensitivities of the 1.3 MHz and 5.2 MHz transducers of an acoustic sediment probe were measured using the backscatter amplitudes from stainless steel wires of four different radii. A two-frequency inversion algorithm estimating the geometric mean radius and variance about the mean of suspended sediment with an assumed lognormal size distribution and the sediment mass concentration was developed and tested in a laboratory setting.

The sensitivity of the 5.2 MHz transducer for each wire was consistent within 10%. The sensitivity of the 1.3 MHz transducer calculated for each wire was not consistent and is believed to be due to a strong angular dependence between the wire orientation and the 1.3 MHz transducer face. The sensitivities of each of the four transducers were, however, inferred from the system's response to the controlled sediment backscatter measurements.

TABLE OF CONTENTS

I. INTRODUCTION

The coastal region of the United States is of high economic, recreational and strategic value. Ports and harbors are important for the import of foreign goods and the export of agricultural and industrial products. The coastal region is subject to many natural forces, often resulting in disastrous consequences. Although storms have important effects on coastal property, the continual exposure of the nearshore zone to waves and currents can have cumulative effects which can be significant over a long period of time. Depending on the wave dynamics and nearshore topography, alongshore littoral drift can cause erosion, transport, and deposition of vast amounts of sediment. The potential for extensive damage to shoreline homes, real estate, and harbor structures exist in both the short and long term. Prediction of sediment transport rates require that the amount of suspended sediment flux be known under a variety of wave conditions. As deep water ocean waves and locally generated wind waves propagate toward the coast, their energy is transformed to higher and lower frequencies in nonlinear interactions under the influence of the underlying topography. The nonlinear fluid motions cause transport of the sediment at the seabed, potentially leading to significant changes in the local topography. Much of the incident wave energy is dissipated by small-scale turbulent motions which strongly couple larger-scale fluid motion through the water column to the sediment bed. Small-scale turbulent kinetic energy is produced at both the surface by non-linear wave interactions and wave breaking, and at the bottom boundary due to shear stress. While the bottom boundary layer is typically only a

1

few centimeters thick under the oscillatory flows found in the nearshore region, under more energetic wave breaking conditions the turbulent boundary layer can occupy the entire water column. Consequently the strong, episodic, multi-scaled forcing in the nearshore region presents unique problems in our understanding sediment transport processes.

Models and measurement of sediment transport in the nearshore must take into account not only the strong irrotational wave motion above the sediment bed, but also the much weaker turbulent motions generated by the fluid flow. Development and verification of models with in-situ data requires high spatial and temporal sampling throughout the water column. Ideally, sediment fluxes should be measured to the smallest turbulent scales throughout the water column to investigate the episodic, non-linear physical processes which produce net sediment fluxes in the nearshore.

Methods of sediment concentration and size distribution measurements range from the physical collection of a volume of suspended sediment and the medium of suspension, to non-invasive methods based on the scatter of incident acoustic or light energy by suspended scatterers. Siphoning of a sample using suction involves the removal of a volume of sediment and medium from the flow without erroneously sampling the sediment bed. This method is restricted by its sensitivity to background currents, particle size, air entrainment, and the direction of suction in relation to the direction of flow (Bosman et al, 1987). Samples are typically siphoned in a direction normal to the flow with a suction velocity which exceeds the ambient flow velocity by more than three times (Bosman et al, 1987), but samples can also be taken along the axis of the flow with a suction velocity which exceeds the maximum settling velocity of the particles under investigation (Hay, 1991). While these

2

methods provide a direct sampling of the concentration, they clearly perturb the flow and are limited in their volume resolution, and extremely limited in temporal resolution.

Transmissometers determine the extinction characteristics of the medium by measuring the attenuation of light along a short light path through the medium. They provide a well controlled sample volume but have limited dynamic range. Empirical models are required to relate the beam attenuation to suspended mass.

Optical backscatter instruments measure turbidity and suspended particle concentrations by detecting scattered infrared radiation. The response of an optical backscatter sensor depends on the size, composition, and shape of suspended particles. This requires calibration with suspensions from the waters to be investigated (D & A Instrument Company, 1991). OBS instruments are well suited to the measurement of suspended concentrations with their wide dynamic range, linear response to increasing concentrations, and insensitivity to bubbles and organic matter. Their primary limitation for small-scale studies is that the sample volume depends on the concentration of the suspended sediments being measured. This leads to a poorly defined sample volume, and so are more suited to the measurement of bulk sediment concentrations.

The use of acoustic backscatter instruments is a promising area of research. Small and robustly engineered acoustic backscatter instruments are well suited to sediment flux measurements. Unlike siphon sampling, the acoustic instrument can be deployed well above the boundary layer (typically 1 meter), directed downward to measure the turbulent boundary layer properties with non-intrusive acoustic beams. Current implementations of this technology have high spatial [O(1 cm)] and temporal resolution [O(0.1 s)] providing a

method for sampling the small-scale concentration levels in the boundary layer (Hay, 1983). Sampling the sediment along the length of the acoustic beam in range bins is accomplished by rapidly sampling received acoustic energy levels from short duration transmitted acoustic pulses. Inversion techniques are used to convert the acoustic backscatter levels to particle concentration and size distribution parameters. This allows measurements of sediment concentration properties spanning the depth of the boundary layer. The inversion technique developed in this study is based on previous work (Hay and Sheng, 1992) utilizing multiple acoustic frequencies.

The acoustic backscatter instrument utilized in this study is the Coherent Acoustic Sediment Probe (CASP) developed under the direction of T. P. Stanton at the Department of Oceanography, Naval Postgraduate School. The CASP is a two-frequency, dual mode underwater instrument package originally designed for the study of surface boundary layer turbulence. It uses three 5.292 MHz transducers and a single 1.323 MHz transducer to determine three components of velocity, suspended sediment concentration profiles, and sediment size distribution using a multi-frequency approach described in the following chapter. By combining the three velocity components measured by the CASP and the sediment concentration estimated from an inversion of the volume backscattered strengths, three components of the sediment flux can be determined down to centimeter scales.

In this study, the absolute sensitivity of the CASP acoustic backscatter system was determined using a fixed wire backscatter calibration technique following the theoretical development by Sheng and Hay (1993). A verification of the two frequency inversion algorithm was made with the CASP using controlled concentrations of sediments collected

from local beaches. Acoustic backscatter data were collected for sub-octave concentrations up to 2.1 g/liter using sorted sediment samples of known lognormal size distributions. A homogeneous sediment suspension of pre-determined mass concentrations was achieved using a uniquely designed test vessel. The test vessel provided a well mixed test volume with an acoustically transparent window and no interior level surfaces which could allow sediment to settle out during the trials. The design also avoided the generation of turbulent vortices and bubble entrainment from the air-water boundary.

The background theory used to determine the sensitivity of the CASP acoustic transmitter/receiver and the sediment inversion technique are presented in Chapter II. The experimental methods used to determine the CASP sensitivity and test the inversion technique are described in Chapter III. Results are discussed in Chapter IV, and are followed by conclusions and recommendations in Chapter V.

II. BACKGROUND THEORY

A. COHERENT ACOUSTIC SEDIMENT PROBE (CASP)

The CASP measures high temporal and spatial resolution acoustic backscatter information to determine the suspended mass, M, and velocity, V, which are used to calculate the total sediment flux vector, $F = M \cdot V(x,y,z,t)$. A theoretical inversion technique is required to convert the backscatter acoustic pressure measurements from the CASP into sediment size distributions and mass concentrations. The amplitude of backscattered acoustic energy at a given frequency depends on the number of scatterers, their size, and their acoustic impedance in the sample volume. For simple particle size distributions, the size *versus* frequency dependence of the scattering cross sections can be used to estimate both the scatterer size and mass concentration by taking backscatter measurements at multiple frequencies. The multi-frequency approach requires knowledge only of the overall sensitivities of the acoustic instruments and of the frequency/size dependence of the scattering cross section of the particles.

An underwater acoustic backscatter instrument requires a transducer to convert transmitter electrical energy into acoustic energy, and to convert received acoustic energy into electrical energy. In the CASP, a transducer of known dimensions is electrically excited to produce a short, high frequency acoustic pulse which propagates through the water. Backscattered energy may be received at the same transducer (monostatic mode), or at a transducer

6

separated in space from the transmitter (bistatic mode). This theoretical treatment focuses on the monostatic mode—the bistatic mode is an extension using a different form factor.

Consider a pulsed, narrow-beam transducer shown in Figure 2.1. The detected volume is in the far field, defined by $r > \pi a_c^2 / \lambda$ (Clay and Medwin, 1977), where r is the distance from the transducer to the detected volume, a_o is the transducer radius, α_0 is the attenuation coefficient in water, α_s is the attenuation due to the suspended particles, and λ is the acoustic wavelength. The sample volume of each acoustic beam is defined across-beam by the -3 dB beam width, $2\beta_0$, and radially by the width of the transmitted pulse length, $c\tau/2$, where c is the sound speed in water, and τ is the duration of the transmitted pulse. The detected volume is the volumetric intersection of the cylindrical sample volumes of the transmitter and receiver acoustic beams. The transducer detects backscattered acoustic pressure, P_s, returned from particles in the transmitted beam path. The particles are assumed to be randomly and homogeneously distributed across the detected volume and the concentration is assumed to be low enough that multiple scattering can be ignored. This assumption is valid when the mass concentration is less than 30 g/L for quartz particles (Varadan et al, 1983). The maximum mass concentration in the series of calibration runs conducted for this study was 2.08 g/l (32 g/15.4 liter), although field measurements could well reach strong scattering values.
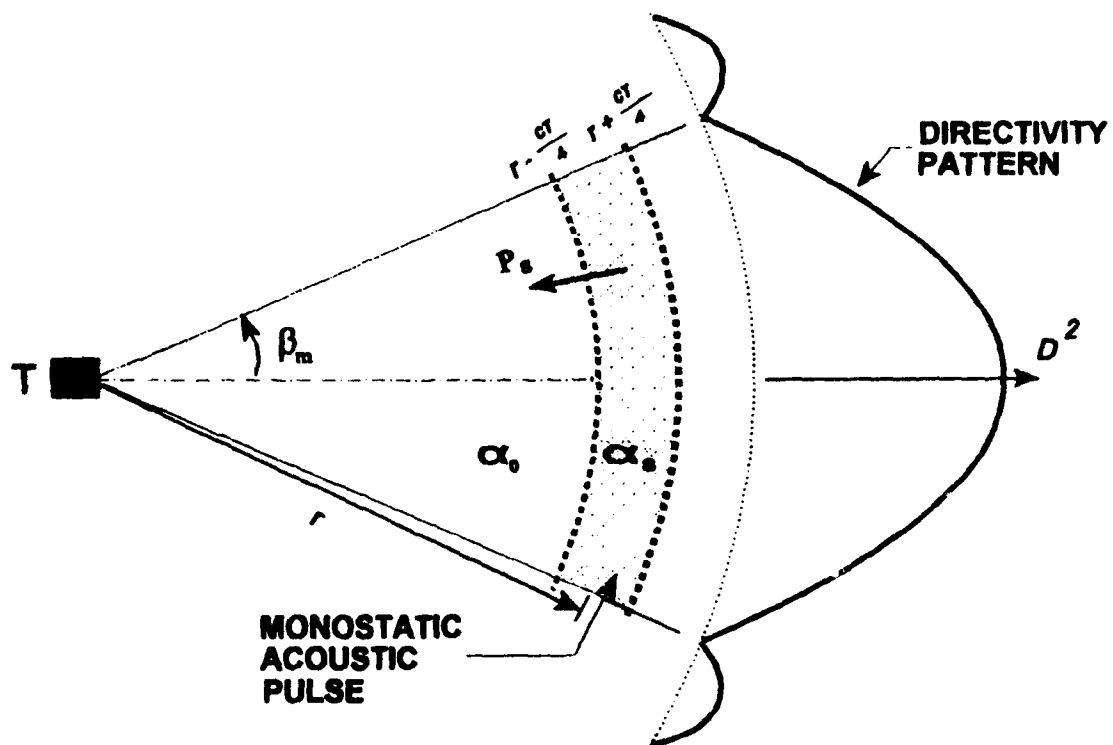
Figure 2.1 Geometry of a pulsed monostatic acoustic system and generalized directivity
pattern showing the main and side lobes of the acoustic beam. T represents the transducer.
The remaining symbols are defined in the text.

B. TRANSDUCER DIRECTIVITY

The farfield directivity, D, for a circular piston transducer of radius a_0 is given by

$$D = \frac{2 J_1(k_C a_0 \sin \beta)}{k_C a_0 \sin \beta} \qquad (2.1)$$

(Clay and Medwin 1977) where J_1 is the cylindrical Bessel function of order 1, and k_C ($= 2\pi \lambda$), the compression wave number. Table 1 contains characteristics of the CASP transducers for a sound speed c = 1480 m/s and a pulse duration $\tau = 2.26 \times 10^{-5}$ sec. The theoretical directivity patterns for the 1.323 MHz and 5.292 MHz acoustic beams are shown in Figure 2.2, in terms of the spreading angle β.

TABLE 1 CASP MONOSTATIC ACOUSTIC BEAM CHARACTERISTICS

Freq. (MHz)	Transducer Radius (cm)	Wave-length (cm)	Farfield Range (cm)	Half Power Beamwidth (deg)	Half Power Beamwidth (cm)	Pulse Length (cm)
1.323	1.27	0.112	45.2	2.62	1.14	1.68
5.292	0.317	0.028	11.3	2.62	1.14	1.68

C. BACKSCATTER RESPONSE TO LOGNORMAL SIZE DISTRIBUTION

The pressure amplitude of incident spherical sound waves in the detected volume can be expressed as (Hay and Sheng, 1992)
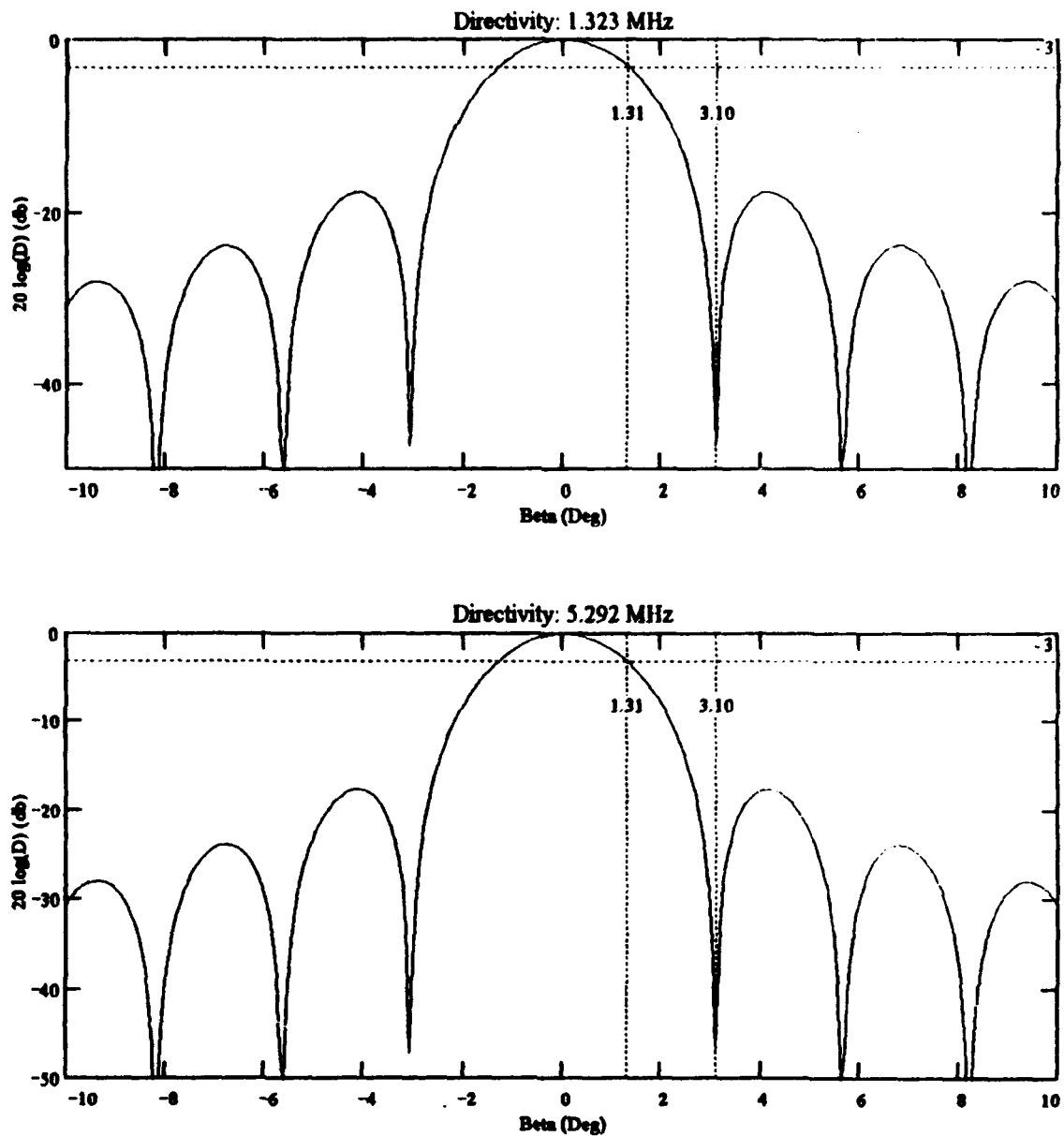
Figure 2.2 CASP 1.323 MHz and 5.292 MHz transducer directivity patterns with angles of the first null point and the half power bandwidth for each frequency shown.

10

$$p_i = p_* r_* \frac{D(\beta)}{r} \exp\left[-\alpha_0 r - \int_0^r \overline{\alpha_s}\, dr\right] \qquad (2.2)$$

where p_* is the on axis pressure amplitude at r_*, the reference distance; r is the distance from the transducer to the detected volume with $r \ll r_*$, α_0 is the attenuation coefficient in clean water, $\overline{\alpha_s}$ is the attenuation due to the suspended particles. The overbar denotes the average over the size distribution. D is the transducer directivity.

Representing the particles as solid spheres of equivalent size and letting $\overline{V}$ be the output voltage of the receiver, it can be shown that (Hay 1991)

$$\overline{V} = \frac{S}{r}\left(\frac{M}{\rho_s}\right)^{1/2} F\left[n(a), f_\infty(x)\right]\left[\frac{\sinh(\zeta)}{\zeta}\right] \exp\left[-2\int_0^r \overline{\alpha_x}\, dr''\right] \qquad (2.3)$$

where

$$\zeta = c\,\tau\,(\alpha_0 + \overline{\alpha_s}) \qquad (2.4)$$

11

and

$$F\left[n(a), f_\infty(x)\right] = k_C^{-1/2} \left[\frac{\int_0^\infty a^2 |f_\infty(x)|^2 n(a)\, da}{\int_0^\infty a^3 n(a)\, da}\right]^{1/2} \qquad (2.5)$$

where S is the overall system sensitivity constant, 1/r is the radial spreading term, a is the equivalent radius of the particle, $n(a)$ is the size spectral density, M is the mass concentration of scatterers, and ρ_s is the grain density of the particle. ζ is the combined attenuation of acoustic energy due to the attenuation effects of the medium and the scatterers in the acoustic beam. $F\left[n(a), f_\infty(x)\right]$ is the response function due to the size distribution and far-field backscatter form factor, $f_\infty(x)$, of the particle. Here, x is given by $x = k_c a$, where k_c is the compression wave number. The term $\left[\sinh(\zeta)/\zeta\right]^{1/2}$ corrects for attenuation across the detected volume (Hay and Sheng 1992).

Most sediment distributions in the nearshore can be represented by a lognormal distribution of the form

$$n(a)\, da = \frac{1}{\sqrt{2\pi}\ln\sigma_g} \exp\left[-\frac{(\ln a - \ln a_g)^2}{2(\ln\sigma_g)^2}\right] d(\ln a) \qquad (2.6)$$

which is characterized by the parameters a_g, the geometric mean radius of the particles, and $(\ln\sigma_g)^2$, the variance of $\ln a$ about its mean. For example, Figure 2.3 shows a best fit
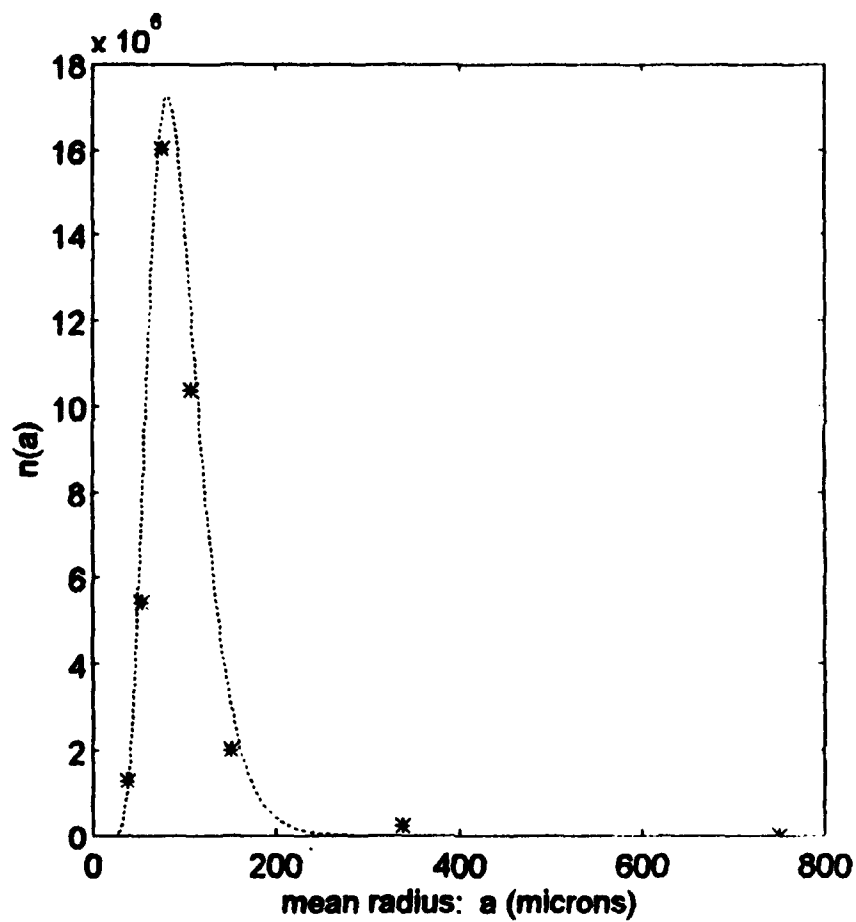
12

Figure 2.3 Best fit comparison between the grain size distribution for Monterey Wharf and a lognormal distribution with $a_g = 82$ microns and $\sigma_g = 1.26$.

13

comparison between the size spectral density for sediment collected at Monterey Wharf and a lognormal distribution with a mean geometric radius of 82 microns and $\sigma_g = 1.22$. The symbols (*) represent the number of grains in each sieve size range assuming each sediment grain has a diameter equal to the mean size of each sieve range. The distributions for Asilomar State Beach and Naval Postgraduate School Beach are similar with values of $\sigma_g = 1.22$, $a_g = 135$ microns and $\sigma_g = 1.22$, $a_g = 94$ microns respectively. This single mode, lognormal distribution is a widely observed sediment size distribution. However, multi-modal distributions can occur, requiring a more elaborate parameterization using a larger number of frequencies and a different form factor than the two frequency approach described here. The form factor for uniformly-sized particles, assuming the particles have a lognormal size distribution, is plotted in Figure 2.4 as determined empirically by Hay (1991) and is expressed

$$|f_\infty(x)| = \frac{1+1.25x^4}{1+x^4} \left[|f_\infty(x)_{rigid, mobile}|^2 \right]^{1/2} \tag{2.7}$$

where $|f_\infty(x)_{rigid, mobile}|$ is the theoretical form factor for a rigid, mobile, spherical particle with the density of quartz (Hay and Mercer, 1985) and $x = ka_g$, where a_g is the mean geometric radius of the particles. The dependence of the form factor on the frequency of the acoustic energy and the size of the particles allows the use of two different frequencies to estimate the size of the particles. The theoretical values of the response function, $F[n(a), |f_\infty(x)|]$, for natural sand particles can be computed assuming a lognormal particle
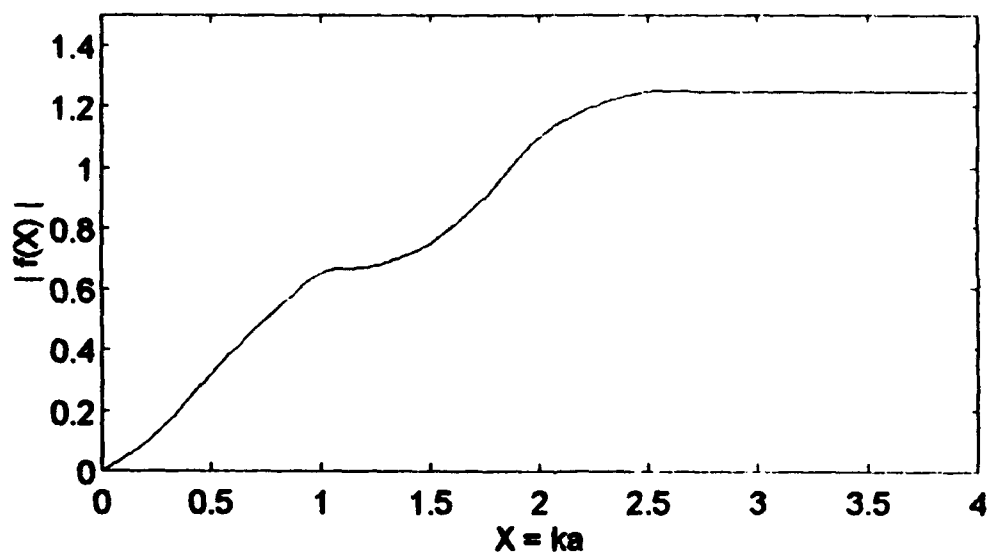
14

Figure 2.4 Empirically determined form factor for uniformly-sized, spherical particles assuming a lognormal particle size distribution.

size distribution and the form factor for a lognormal size distribution, $|f_\infty(x)|$. Figure 2.5 shows the form of the response function, given by Equation (2.8) below, for each frequency and values of σ_g ranging from 1.1 to 1.5.

After substituting the lognormal distribution into Equation (2.5), $F[n(a),|f_\infty(x)|]$ is now dependent only on a_g, σ_g, and k_c. By letting $X = k_c a_g$,

$$R(X, \sigma_g) = F[n(a), |f_\infty(x)|] = k_c^{-1/2} \left[\frac{\int_0^\infty a^2 |f_\infty(x)|^2 \exp\left[-(\ln a - \ln a_g)^2/2 (\ln \sigma_g)^2\right] d\ln a}{\int_0^\infty a^3 \exp\left[-(\ln a - \ln a_g)^2/2 (\ln \sigma_g)^2\right] d\ln a} \right]^{1/2} \quad (2.8)$$

Assuming the scattering attenuation is small, or has been completely corrected for, the backscatter for the two frequencies can be expressed by

$$K_C = S_i (M/\rho_s)^{1/2} F(X_i, \sigma_g) \quad i = 1, 5 \quad (2.9)$$

where the subscript i represents the 1.3 and 5.2 MHz frequencies. The ratio of the relationship in Equation (2.9) for each frequency can be expressed as (Hay and Sheng 1992)

$$\frac{F(X_5, \sigma_g)}{F(X_1, \sigma_g)} = \frac{S_1}{S_5} \frac{K_{C_5}}{K_{C_1}} \quad (2.10)$$

which eliminates the dependence on M, the mass concentration. The right-hand side can be evaluated from measurements of the sensitivity S, and the digital output, K_c, from a
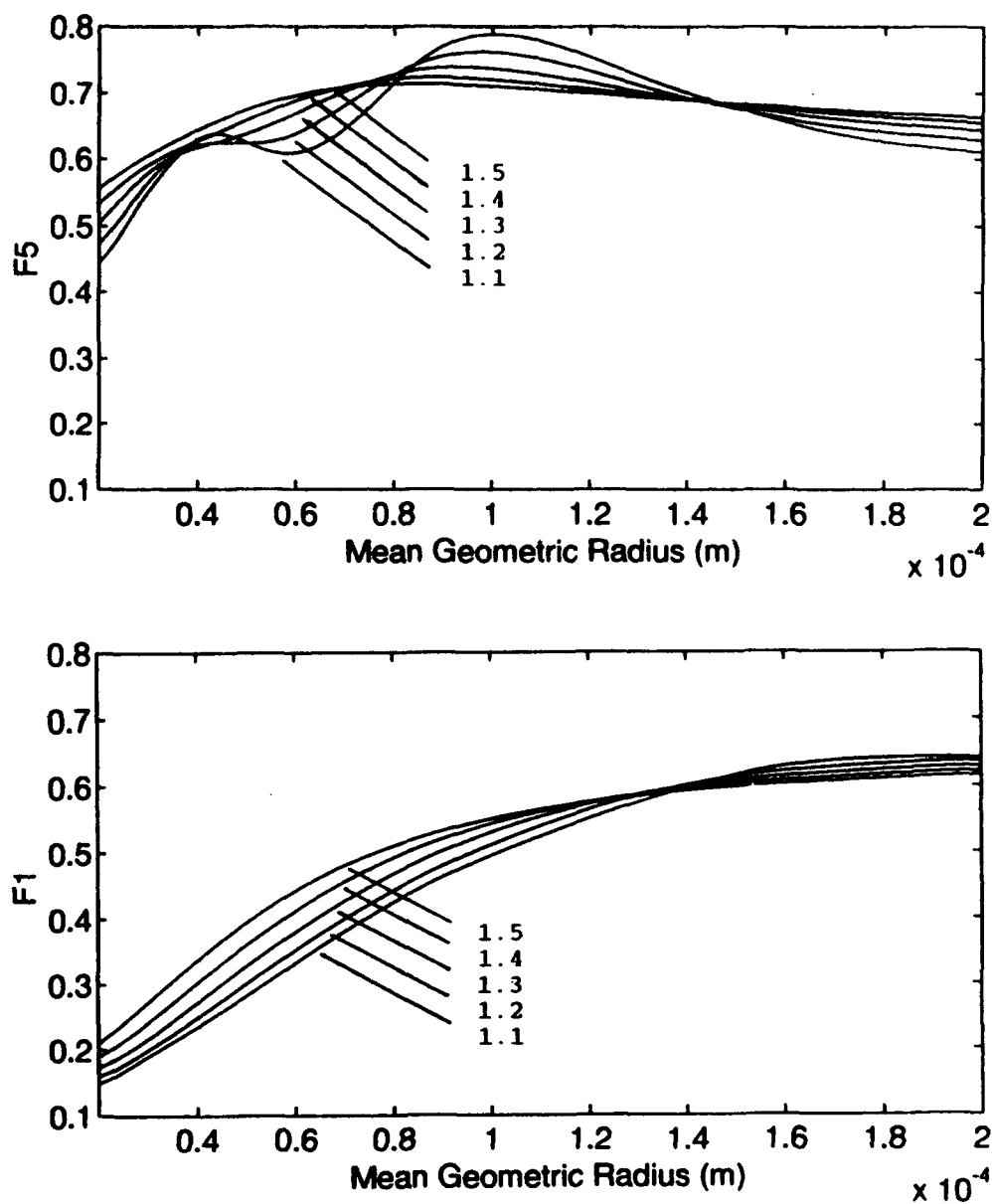
16

Figure 2.5 Response functions for 1.323 MHz and 5.292 MHz, assuming a lognormal particle size distribution, as a function of the particle mean geometric radius for values of $\sigma_g = 1.1, 1.2, 1.3, 1.4, 1.5$.

lognormal sediment sample. The left-hand side of the equation can be evaluated using Equation (2.7) using the expression for $|f_\infty(x)|$. Figure 2.6 shows the theoretical form of the ratio $F(X_s, \sigma_g)/F(X_1, \sigma_g)$. Using only two frequencies, it is not possible to determine both a_g and σ_g, so the value of the lognormal distribution variance parameter σ_g must be prescribed. Theoretically the value of σ_g can be determined in methods using more than two frequencies, but the inherent statistical noise of the backscatter measurements is large enough to make the σ_g estimates vary widely, so σ_g must be prescribed (Hay and Sheng, 1992). Based on the values of σ_g determined for the sediment samples collected at the three locations mentioned above, a value of $\sigma_g = 1.2$ is used in this study. In field studies, the value of σ_g will be estimated from a lognormal distribution analysis of a sediment sample from each location of interest.

To estimate the mean geometric particle radius of the sediment, the measured ratios calculated from the right-hand side of Equation (2.10) are compared with the theoretical ratios of $F(X_s, \sigma_g)/F(X_1, \sigma_g)$. In practice, the estimate of a_g is obtained from a match to the value of the $F(X_s, \sigma_g)/F(X_1, \sigma_g)$ function which is stored in a lookup table in the analysis software.

The mass concentration in the same range bin can be estimated by explicitly solving Equation (2.9) for M,

$$M = \frac{\rho_s}{2} \left[\frac{K_{C_1}^2}{S_1^2 F^2(X_1, \sigma_g)} + \frac{K_{C_s}^2}{S_s^2 F^2(X_s, \sigma_g)} \right] \qquad (2.11)$$
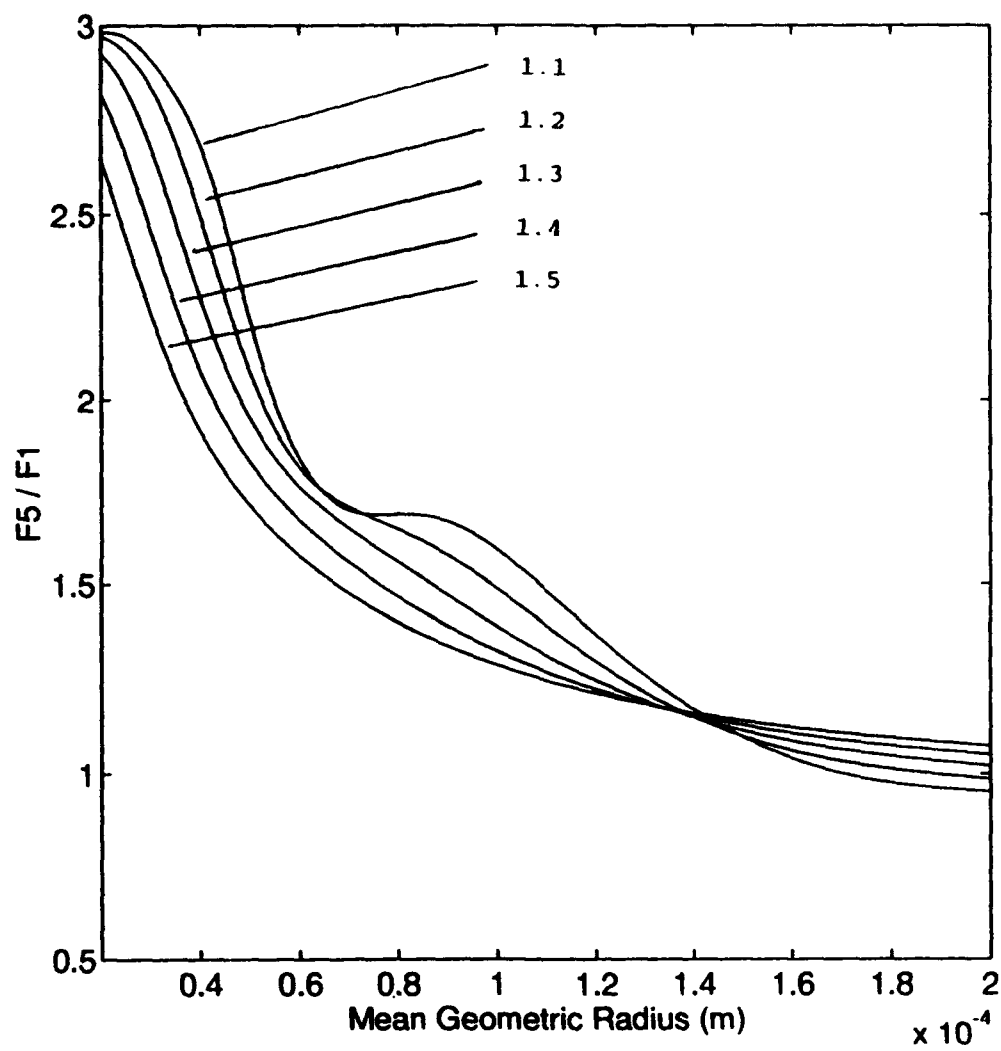
Figure 2.6 Theoretical values of $F(X_5, \sigma_g)/F(X_1, \sigma_g)$ as a function of a_g for $\sigma_g = 1.1, 1.2, 1.3, 1.4, 1.5.$

where ρ_s is the density of the scatterers, K_c is the digital backscatter counts for each frequency, S is the sensitivity for each frequency, and $F(X, \sigma_g)$ is calculated from Equation (2.10).

This method therefore provides a technique for estimating mass concentration and the mean geometric particle radius from the dual frequency backscatter levels and the assumed lognormal sediment distribution standard deviation parameter σ_g. A method for determining the system sensitivity, S, for each frequency of the CASP is discussed next.

D. SYSTEM SENSITIVITY

Following the theoretical development of Sheng and Hay (1993), the estimate of the sensitivity for a frequency using wires, S_w, can be expressed as

$$S_w = \frac{1}{r} \frac{\sum_{i=1}^{4} \left[K_c \, |\Gamma_p| \frac{\sqrt{x_i} |f_\infty(x_i)|}{\sqrt{2kr}} \right]}{\sum_{i=1}^{4} \left[|\Gamma_p|^2 \frac{x_i |f_\infty(x_i)|^2}{\sqrt{2kr}} \right]} \tag{2.12}$$

where r is the perpendicular distance from the transducer to the wire, 1/ r is the radial spreading term, K_c are the digital counts of the backscatter amplitudes, and k is the compression wave number. The index of summation, i, is determined by the number of different sized standard targets used. Four stainless steel wires of different diameters were used in this study.

For a pulsed wave acoustic source, the function Γ_p describes the dependence of the backscatter amplitude on the effective length of the wire and is expressed by (Sheng and Hay, 1993)

$$\Gamma_p(r_0) = \sqrt{\frac{2kr_0}{\pi}} e^{-i(\pi/4)} \int_{\beta_1}^{\beta_2} D^2 \exp\left[2ikr_0\left(\sec\beta - 1\right)\right] d\beta \qquad (2.13)$$

where β_1 and β_2 are functions of r_1, the distance to the leading edge of the acoustic wave front, and r_0 is the perpendicular distance from the transducer to the fixed wire,

$$\beta_1 = 0, \quad \beta_2 = \arccos(r_0/r_1), \quad r_0 \le r_1 \le r_0 \sec\beta_m,$$

$$\beta_1 = 0, \quad \beta_2 = \beta_m, \quad r_0 \sec\beta_m \le r_1 \le r_0 + \tfrac{1}{2}c\tau$$

A schematic of the coordinate system for the pulsed system is shown in Figure 2.7. Figure 2.8 shows Γ_p as a function of the parameter $\psi(r_0)$, the ratio of the radius of the main lobe of the transducer directivity pattern, $r_0 \tan\beta_m$, to the radius of the first Fresnel zone

$$\psi(r_0) = \frac{r_0 \tan\beta_m}{\sqrt{\frac{1}{2}r_0 \lambda}} = \frac{\sqrt{kr_0}}{\pi} \tan\beta_m \qquad (2.14)$$

where ψ depends on the acoustic frequency and beamwidth. The values of $\psi(r_0)$ and Γ_p for the 1.3 MHz and 5.2 MHz transducers in this study are 0.98, 0.5; and 2.2, 0.7 respectively.
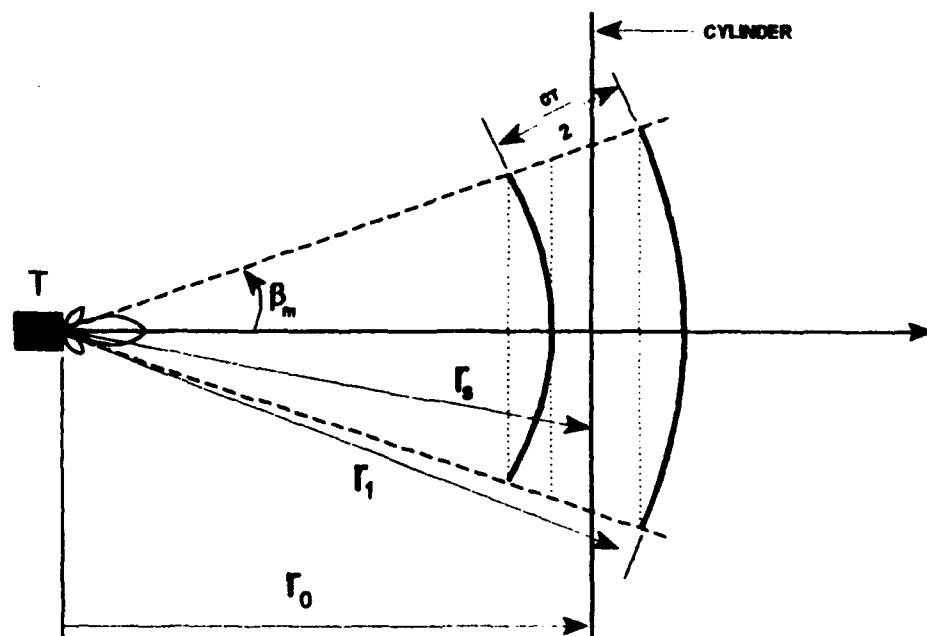
21

Figure 2.7 Schematic of the coordinate system used for an acoustic pulse incident on a fixed wire of infinite length. T represents the transducer. The other symbols are explained in the text.
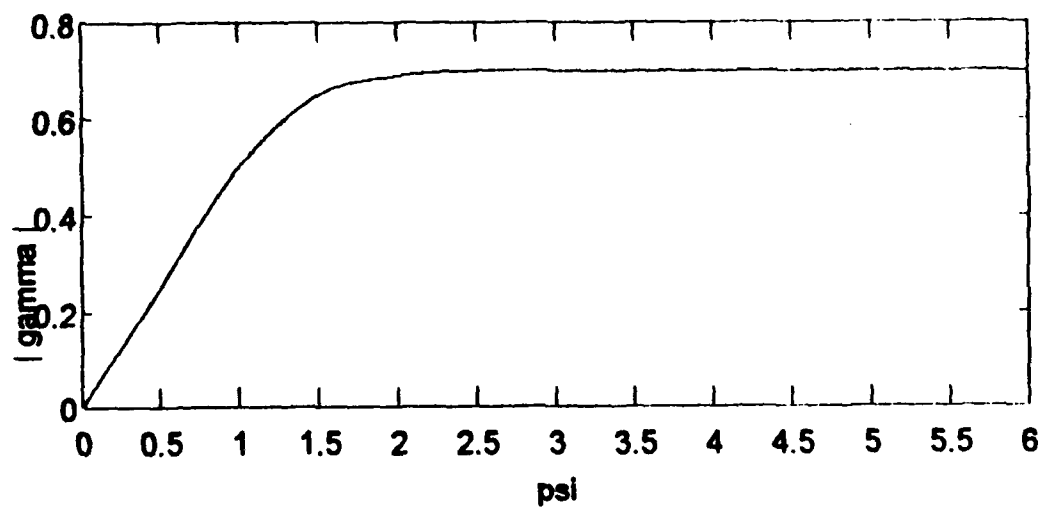
Figure 2.8 Γ_p as a function of $\psi(r_0)$ for a monostatic pulsed acoustic system.

The form factor for an infinite cylinder, $f_\infty(x)$, can be expressed by (Sheng and Hay, 1993)

$$f_\infty(x) = -\frac{2i}{\sqrt{\pi x}} \sum_{n=0}^{\infty} (-1)^n \epsilon_n \sin \eta_n \exp(-i\eta_n) \qquad (2.15)$$

where the Neumann factor $\epsilon_n = 1$ for $n = 0$ and $\epsilon_n = 2$ for $n \geq 1$, and η_n is the phase shift of the nth partial wave (Faran, 1951). Figure 2.9 shows the dependence of the form factor on the acoustic frequency and the radius of the wire. Table 2 lists the values of ka_g and $f_\infty(x)$ for this study.

TABLE 2 VALUES OF ka_g AND $f_\infty(x)$ FOR EACH FREQUENCY AND WIRE RADIUS

Wire Radius (microns)	1.323 MHz		5.292 MHz	
	ka_g (m^{-1})	$f_\infty(x)$	ka_g (m^{-1})	$f_\infty(x)$
25	0.14	0.12	0.56	0.74
40	0.22	0.22	0.90	0.92
50	0.28	0.32	0.12	0.81
64	0.36	0.44	1.44	0.72

The relationship of $f_\infty(x)$ to ka for 1.3 MHz is generally linear while the relationship for 5.2 MHz shows the values of $f_\infty(x)$ increase for the first two values of ka then decrease for the remaining two value. This frequency/target size dependency of $f_\infty(x)$ allows the use of a multi-frequency approach to discriminate between different sized targets.
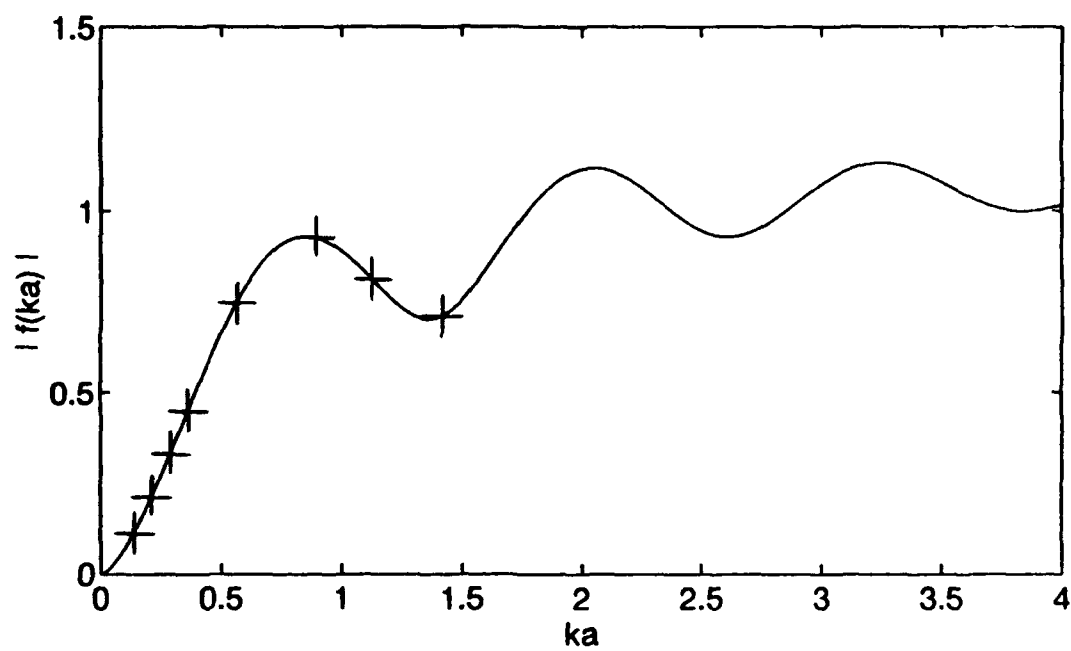
Figure 2.9 Form factor for an infinite cylinder. The values for the 1.3 MHz and 5.2 MHz and wire size combinations used in this study are shown.

III. LABORATORY ACOUSTIC BACKSCATTER MEASUREMENTS

The absolute backscatter sensitivity for each frequency of the CASP was calculated using the procedure discussed in Section II D. The standard targets, four stainless steel wires of different diameters, were suspended in a 600 gallon tank while the primary sample volume of the CASP was moved through a grid of points centered on the wire. The CASP was paused at each grid point and backscatter levels were measured to calculate the sensitivity for each frequency. The backscatter levels were also used to compare the monostatic beam characteristics of the angular width of the first null point, half power bandwidth, and pulse length to theoretical values.

The inversion technique discussed in the previous chapter was verified by developing a method to measure the backscatter levels of known sediment concentrations in a unique test vessel. Clean and sorted sediment samples of increasing cumulative weight were placed into a known volume of water in a test vessel. The sediment was suspended by continuous stirring, then ensonified by the CASP to measure the backscatter levels from the increasing concentrations.

A. COHERENT ACOUSTIC SEDIMENT PROBE (CASP)

The CASP is a robustly constructed, multi-frequency, underwater instrument package originally designed to conduct studies of turbulence in the surface boundary layer. It has three 5.2 MHz acoustic transducers placed radially around a single 1.3 MHz transducer, a

two axis tilt sensor, and a three axis accelerometer to detect the instrument's orientation and motion. In the bistatic mode, one of the three 5.2 MHz transducers emits a series of 32 short (0.5 cm) pulses into the water column, while the other two transducers receive the backscattered acoustic energy from the sample volume defined by the intersection of the transmitter and receiver beams. After 32 backscattered pulses have been sampled by both receiving transducers, the transducers are electronically switched so another 5.2 MHz transducer emits a pulse and the other two receive. The monostatic sampling mode is interleaved into the bistatic sampling sequence to estimate the along-beam backscatter intensity for the three 5.2 MHz transducers and the single 1.3 MHz transducer. In the monostatic mode, a triplet of longer (1.68 cm) pulses are transmitted from each transducer in sequence. As each pulse is transmitted, the transducer is switched to the receive mode and the backscatter amplitudes are sampled in each 1.68 cm range bin out to 1.2 meters. The complete sequence of three bistatic and three monostatic transmit modes is continuously repeated at a rate of 35 Hz (Stanton, 1993).

The 1.3 MHz transducer is mounted flush in the center of the CASP instrument head, and the 5.2 MHz transducers are mounted on 10 cm arms arranged radially outward from the instrument head at 0°, 120°, and 240° (where 0° denotes the top of the instrument head). Figure 3.1 illustrates the acoustic beam geometry of both the bistatic and monostatic modes. The four acoustic beams intersect at a primary sample volume 25.4 cm downbeam from the 1.3 MHz transducer.
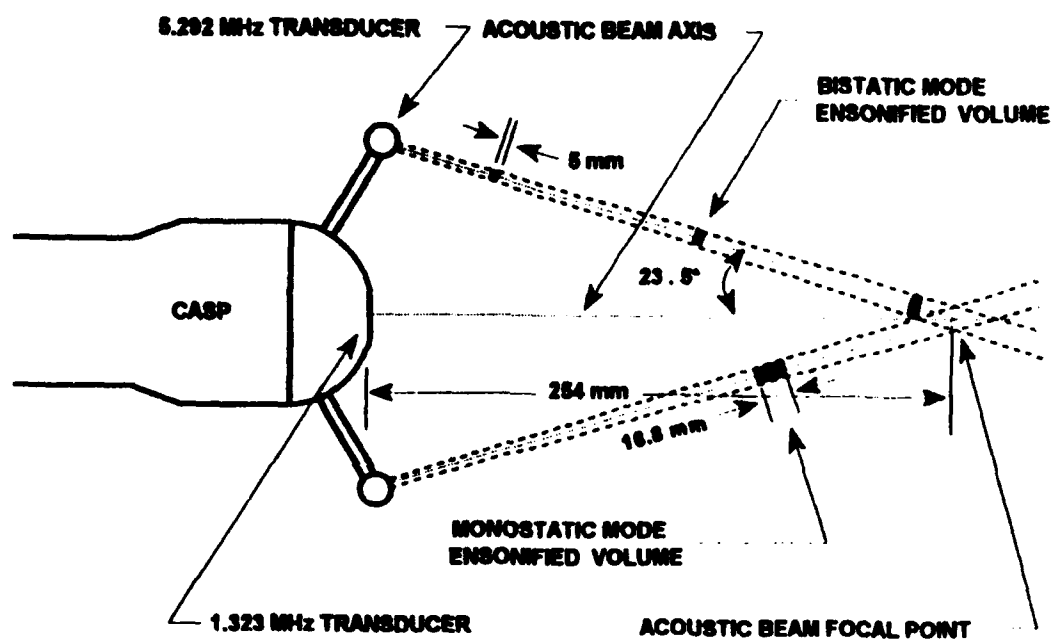
Figure 3.1 Schematic of the CASP acoustic beam geometry for the bistatic and monostatic modes. (Stanton 1993)

B. ABSOLUTE BACKSCATTER SENSITIVITY

The absolute system response of the CASP to backscatter from cylindrical targets of known diameter was calculated following the procedure discussed in Section II D. Previous studies have been based on spherical targets, particularly lead-glass beads. Spheres have the advantage that their target strength is independent of orientation, but it can be difficult to suspend a spherical target precisely in the center of the acoustic beam, particularly in the very narrow acoustic beams generated by transducers operating at MHz frequencies. Wire targets offer the advantage that the mounting structure is located completely outside the acoustic beam path so backscatter from the supporting structure is not present.

Sheng and Hay (1993) conducted a study comparing system sensitivity calculations using lead-glass beads with those calculated using stainless steel wires. There was good agreement between the two approaches when an appropriate correction factor was made, indicating that stainless steel wires can be used as standard targets in system sensitivity calculations.

In this experiment, system sensitivity was determined using stainless steel wires of four different radii: 25, 40, 50, and 64 microns. Table 3 lists the values of x (= $k_c a$) for c = 1480 m/s for each wire and frequency combination. The values of k_t for the 1.3 MHz and 5.2 MHz transducers were 5617 m^{-1} and 22467 m^{-1} respectively.

TABLE 3 RADII AND VALUES OF x = ka (m⁻¹) FOR EACH FREQUENCY AND WIRE COMBINATION

Radius (µM)	1.323 MHz	5.292 MHz
25	0.14	0.56
40	0.22	0.90
50	0.28	1.12
64	0.36	1.44

Each wire was suspended under tension in the test tank. The wires were oriented parallel to the transducer face which was being investigated (vertical for 1.3 MHz, 23.5° from the vertical for 5.2 MHz). The CASP was moved under computer control in small increments in X/Y space by a digital servo controller which positioned a precision stage supporting the CASP. The servo controller is capable of incremental movements of the CASP staging as small as 30 microns. The focal point of the acoustic beams traced a grid of points with the wire located approximately in the grid center. Backscatter levels were measured by the CASP at each grid point for a specified period of time. Figure 3.2 shows a plan view of the gird of points used in the absolute backscatter runs. The grid dimensions in these calibrations were 5 cm by 10 cm with an increment of 0.2 cm. The dwell time at each grid point was 10 seconds.
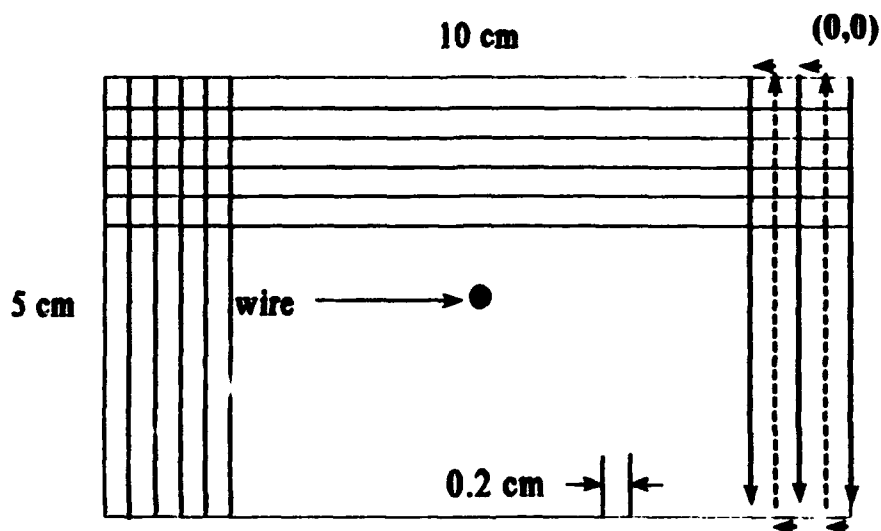
Figure 3.2 Plan view of the 5 cm by 10 cm grid traced out by the primary sampling volume of the CASP during the absolute backscatter runs. The data collection run began with the primary sampling volume in the (0, 0) position with the arrows indicating the motion of the CASP. The solid arrows indicate data collection, while the dashed arrows indicate repositioning of the CASP in increments of 0.2 cm.

C. LABORATORY SEDIMENT BACKSCATTER TESTS

1. Experimental Tank and Mixing Vessel

A 600 gallon acrylic tank was used to contain the CASP in fresh, filtered water during the calibration procedures. The tank was equipped with a computer-controlled X/Y positioning stage under which the CASP was suspended. The relative size of the tank and the CASP (Figure 3.3) allowed targets to be positioned in the path of the acoustic beams as the CASP stage was repositioned. An acrylic test vessel was constructed with a plastic film window to minimize attenuation across the vessel-water boundary. A controllable speed, vertically oriented propeller stirrer was positioned in a vertical acrylic cylinder serving as a directional nozzle which was secured to the tank frame to center it in the mixing vessel. The mixing vessel and propeller stirrer nozzle were designed so that no level surfaces or flow stagnation points were present which could allow sediment to settle out of the mixing volume and reduce the test sample concentration. The mixing vessel, containing 15.4 liters of clean, deaerated water, was placed in the test tank with an OBS inserted in an O ring sealed sidewall opening with the transducer face positioned downward. The temperature of the tank and mixing vessel water were measured to 0.1° C accuracy. The tank and vessel temperatures differed by at most 1° C throughout the series of test runs. Any bubbles on the CASP or mixing vessel surfaces were brushed off, with particular care being taken around the transducer faces and mixing vessel window. The CASP was positioned such that the acoustic beam intersection point was approximately 1.0 cm inside the mixer vessel window. The propeller stirrer nozzle was placed downward within one degree of vertical in the test vessel and secured to the tank frame. The calibration run for each grain size range was
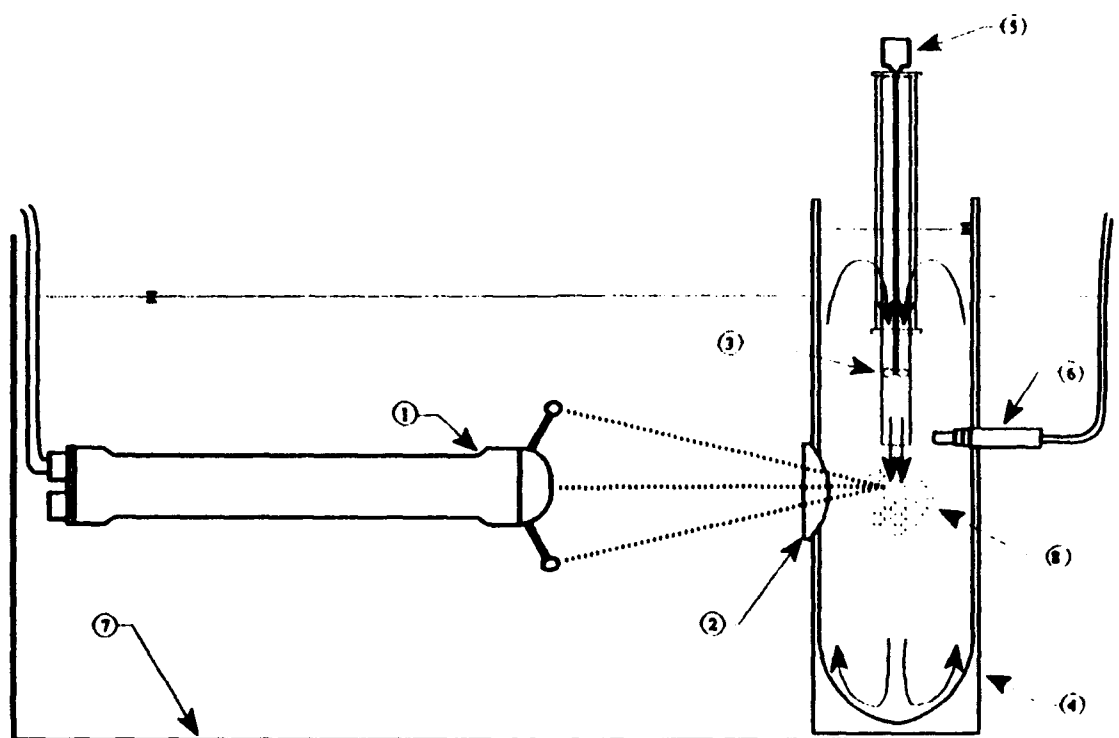
1. COHERENT ACOUSTIC SEDIMENT PROBE (CASP)
2. ACOUSTICALLY TRANSPARENT MEMBRANE
3. ACRYLIC NOZZLE AND DUCTED PROPELLER
4. ACRYLIC TEST VESSEL
5. VARIABLE SPEED MOTOR
6. OPTICAL BACKSCATTER SENSOR
7. ACRYLIC LABORATORY ACOUSTIC TEST TANK
8. SUSPENDED SEDIMENT

Figure 3.3 Schematic of the test tank, CASP, and the mixing vessel with propeller stirrer. (Stanton, 1993)

33

performed by adding sediment samples to the test vessel with the propeller stirrer running, resulting in a homogeneous mass concentration. An equal amount of clear water from the vessel was removed in the sample vial to maintain the mass concentration for that particular run. Backscatter data were collected for 120 seconds. The sorted samples were added to the vessel in sequence, with the final weight of sediment in the test vessel totaling 32 grams. This gave a maximum mass concentration of 2.08 g/l.

2. Sediment Collection and Preparation

Sediment samples were obtained from three locations along the Monterey Bay coast: Asilomar State Beach, Naval Postgraduate School Beach, and the Monterey Wharf. Samples from each location were cleaned, sorted, and weighed to 0.01 gram accuracy. Sieves with mesh sizes of 0.090 mm, 0.125 mm, 0.180 mm, 0.250 mm, 0.355 mm, 1.00 mm, and 2.00 mm were used in the sorting of the samples. Discrete samples of clean and sorted sediment were weighed into vials containing a weak solution of water and Triton 100. Sorted samples were weighed out such that sequential additions of the sediment samples into the test vessel resulted in cumulative sub-octave weights of 0.5, 1.0, 1.5, 2.0, 4.0, 6.0, 8.0, 12.0, 16.0, 24.0, and 32.0 grams. Triton 100 is a wetting agent that prevented the sediment grains from being encased in air bubbles which could significantly increase the backscatter cross section resulting in erroneous backscatter levels.

Backscatter data were analyzed from the first range bin inside the mixing vessel window. Figures 3.4, 3.5, and 3.6 show the mean monostatic backscatter levels for each range bin over the duration of the sample run (120 sec). The left and right panels show the
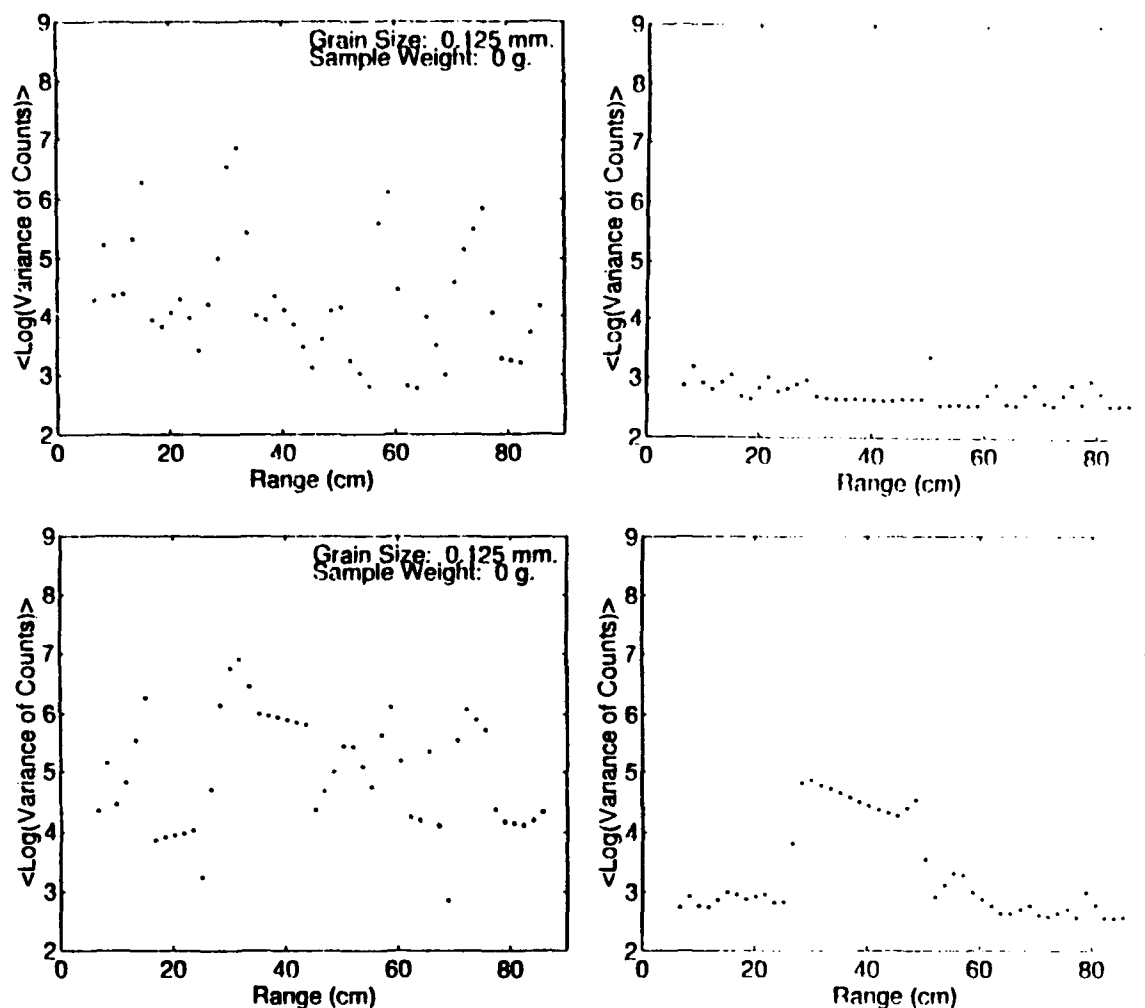
34

Figure 3.4 Mean monostatic log backscatter power level profile for sediment of size 125 to 180 microns. The top panel shows mean backscatter levels for no sediment and no stirring of the mixer vessel water volume. The bottom panel shows mean backscatter levels for no sediment with stirring of the mixer vessel water volume. The left panel shows the backscatter level profile for 1.3 MHz. The right panel shows the backscatter level profile for 5.2 MHz.
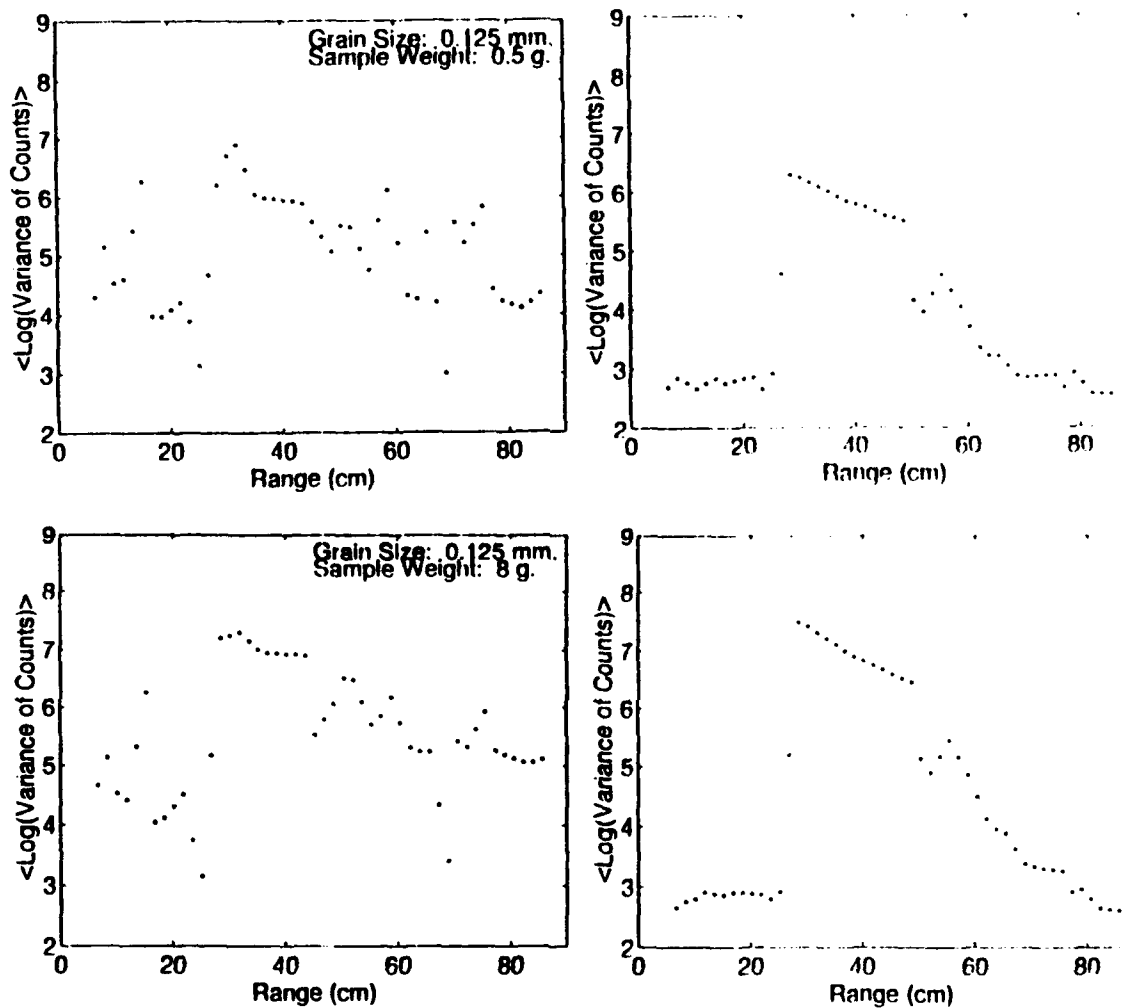
35

Figure 3.5 Same as Figure 3.4 but for 0.5 g and 8.0 g of sediment in suspension.
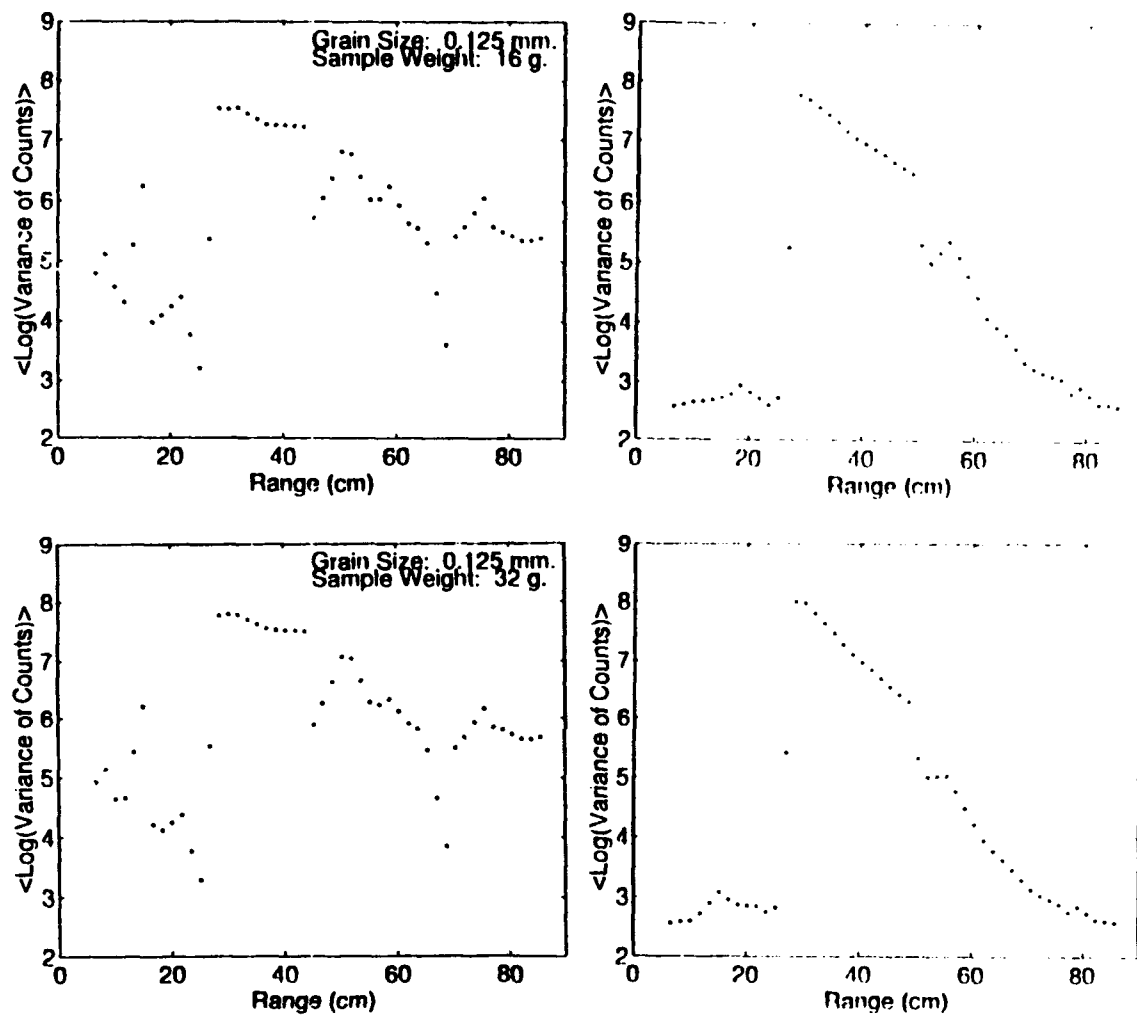
36

Figure 3.6 Same as Figure 3.4 but for 16.0 g and 32.0 g of sediment in suspension.

backscatter levels for the 1.3 MHz and 5.2 MHz acoustic beams respectively for the grain size diameter range of 125 to 180 microns. The cumulative sample weight of sediment shown are 0 grams with no mixing of the water volume, and 0, 0.5, 8.0, 16.0 and 32.0 grams with mixing of the water column. For both the 1.3 and 5.2 MHz frequencies, the 0 gram, no mixing case exhibits backscatter levels which can be attributed to micro-turbulent vortices and small contaminants present in the test tank and mixer water volumes which represent a noise floor for this calibration method. For the mixing cases the 5.2 MHz profiles show a large increase in backscatter power (by a factor of 10^5 for 32 grams) in the mean backscatter power returns inside the mixer window (starting at 26 cm range) at each concentration. The mean backscatter returns for the 1.3 MHz beam also increase inside the mixer window (by a factor of nearly 10^4 for 32 grams) for the higher concentrations but continue to increase for the lower concentrations, to reach a maximum at a range of about 32 cm. The backscatter drops off sharply at about 34 cm where the backscatter profile resembles more closely that of the 5.2 MHz acoustic beam. The higher values of backscatter levels for the low concentration profiles for 1.3 MHz near the 20-25 cm range are believed to be due to the plastic film window. Backscatter values are sampled in the range bins through the suspended sediment volume.

Appendix A contains the sieve analysis for each of the nine samples using the measured weights for each sieve size range. The analyses show the size distributions were significantly different for each of the three locations. The mean percentages of sediment size ranges for the three collection sites shown in Table 4 indicate NPS Beach Lab sediment consists mainly of medium and fine sized silts with most sediment between 0.063 and

0.5 mm. Monterey Wharf sediment is similar to the sediment collected at Asilomar but has a more even proportion of larger sized grains in the 0.5 to 1.0 mm range.

TABLE   PERCENTAGE WEIGHT BY SEDIMENT CLASSIFICATION

Classification	Size Range (mm)	Asilomar	Beach Lab	M. Wharf
Gravel	> 1.0	17.02	0.00	19.35
Coarse Sand	0.500 - 1.0	25.81	1.26	15.04
Med./Fine Silt	0.063 - 0.500	56.15	97.16	64.09
Coarse-Fine Silt	< 0.063	1.02	1.58	1.52

IV. RESULTS AND DISCUSSION

The objectives pursued in this study were the determination of the sensitivity of each frequency of the CASP, and development and verification of a two-frequency algorithm inverting backscattered acoustic energy from a volume of suspended sediment to estimate mass concentration and a geometric mean radius of the suspended sediment. The inversion assumes the sediment is described by a lognormal size distribution with a prescribed variance of the distribution about the mean radius. The system sensitivity for each frequency was determined from the backscatter levels of four stainless steel wires of known diameters using the procedure outlined in Section III B. Directivity pattern characteristics obtained from graphical analysis of the backscatter levels from the four wires were compared to the theoretical values of the monostatic mode for each CASP frequency.

A. WIRE TARGET SYSTEM SENSITIVITY ESTIMATION

The system sensitivity for the CASP was determined by ensonifying each wire separately, following the procedure discussed in Section III B. Table 5 lists the rms counts, the values of ka, the form factor, the sensitivity for each wire; and the overall sensitivity calculated for the 1.3 MHz transducer. Table 6 lists the same information for the 5.2 MHz transducer. From Table 5 and Table 6, the values of ka ranges from 0.14 to 0.36 for 1.3 MHz and 0.56 to 1.44 for 5.2 MHz. The form factor has the range of values of x from 0.14 to 0.36 and is generally linear, as is the plot of peak count values for 1.3 MHz. The form factor for the

40

TABLE 5 PARAMETERS FOR 1.323 MHZ SENSITIVITY CALCULATIONS

	1.323MHz			
Wire Radius (microns)	25	40	50	64
RMS Counts	1694±92	6194±174	19929±1066	30500±2770
X_i (= ka)	0.14	0.22	0.28	0.36
$|f(\epsilon)|$	0.12	0.22	0.32	0.44
Numerator (counts)	0.68	5.75	30.1	71.7
Denominator (10^{-6})	0.16	.86	2.28	5.52
S (10^6 counts)	4.23±0.30	6.67±0.33	13.2±0.92	13.0±1.43
<N>	108.2			
<D> (10^{-6})	8.8			
S_w (10^6 counts)	9.28±5.28			

TABLE 6 PARAMETERS FOR 5.292 MHZ SENSITIVITY CALCULATIONS

	5.292MHz			
Wire Radius (microns)	25	40	50	64
RMS Counts	10922±884	20557±3575	17108±1444	16395±1186
X_i (= ka)	0.56	0.90	1.12	1.44
$|f(\epsilon)|$	0.74	0.92	0.81	0.72
Numerator	37.77	111.78	91.58	88.26
Denominator (10^{-6})	11.96	29.57	28.65	28.65
S (10^6 counts)	3.16±0.28	3.78±0.68	3.20±0.29	3.05±0.24
<N>	329.4			
<D> (10^{-6})	99.2			
S_w (10^6 counts)	3.30±0.70			

41

range of value for 5.2 MHz increases to a relative maximum at a value of x at about 0.85, then decreases to a relative minimum at a value of x of about 1.4.

The rms count values for each frequency and wire combination are plotted in Figure 4.1. The sensitivity values of each wire and frequency combination are plotted in Figure 4.2. Theoretically, the sensitivity for each wire and a single frequency should be the same since the form factor would normalize the different response from wires of different radii. The plot of the 5.2 MHz sensitivities for the four wires shows this is the case, with the sensitivities consistent to 21%. The sensitivities for the 1.3 MHz transducer however are widely spread, suggesting a problem with the measurement procedure. It is suspected that there is a strong dependence between the angle made between the wire and the transducer face and the backscatter response, despite attempts to keep the wires orthogonal to the transducers. The wide range of values for the 1.3 MHz transducer prevented further use of the wire-derived sensitivity values. In future work, a spherical target calibration will be attempted, although it introduces a vertical dependence to the backscatter values.

B. MULTI-FREQUENCY INVERSION ALGORITHM

Thirteen mass concentrations for sediment collected from Monterey Wharf were used to test the CASP response to a known sediment size distribution and controlled concentrations. Figures 4.3 shows the mean monostatic backscatter level profile for each range bin averaged over the duration of the run for a mass concentration of 0.26 g/l. The top panel shows the profile for the 1.3 MHz transducer while the bottom panel shows the profile for the 5.2 MHz transducer. Figure 4.4 shows the profile for a mass concentration of 2.1 g/l. Regression
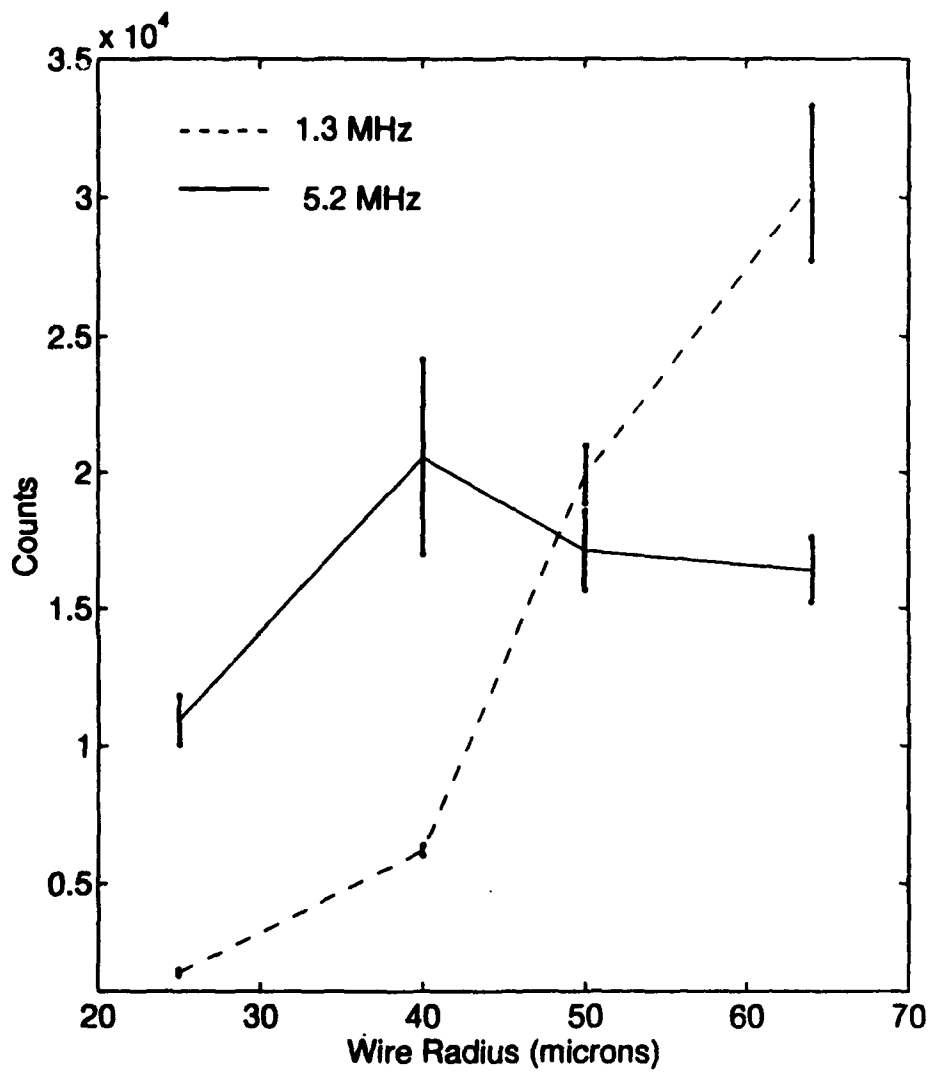
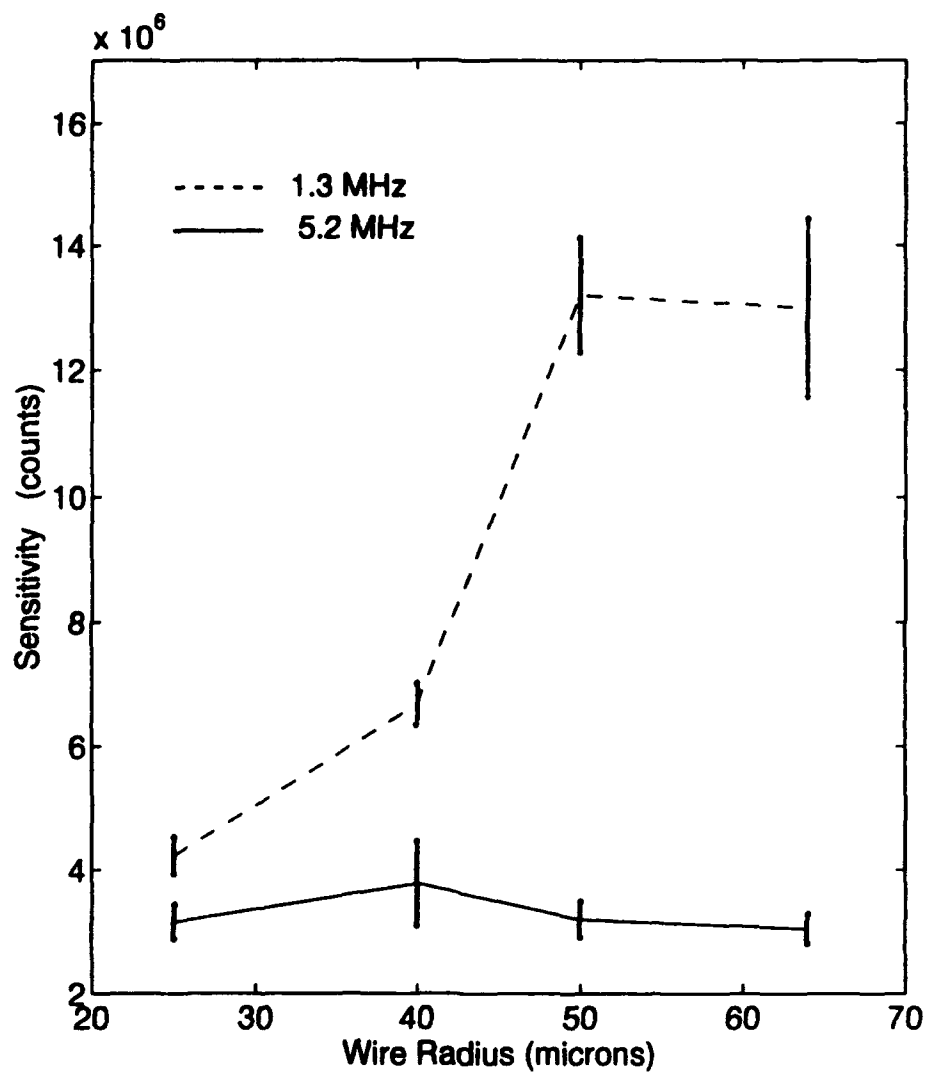Figure 4.1 RMS counts for each wire and frequency combination

Figure 4.2 Sensitivity values for each wire and frequency combination
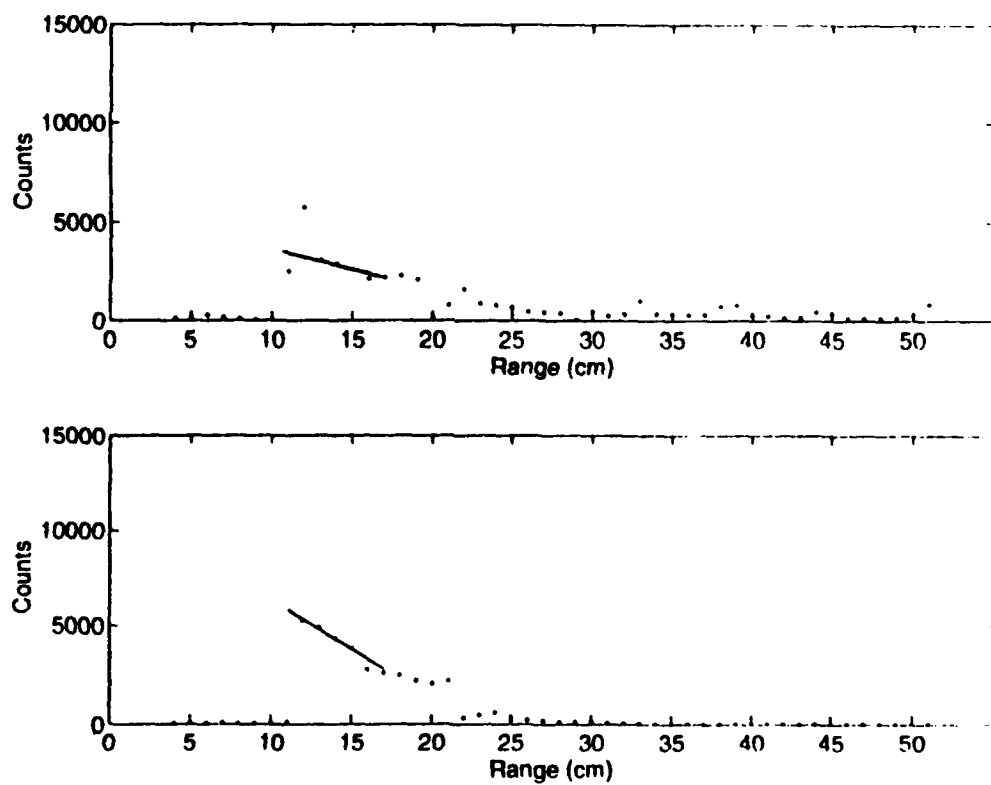
Figure 4.3 Monostatic backscatter level profile for each range bin for a mass concentration of 0.26 g/l. The top and bottom panels show the profiles for the 1.3 MHz and 5.2 MHz transducers respectively.
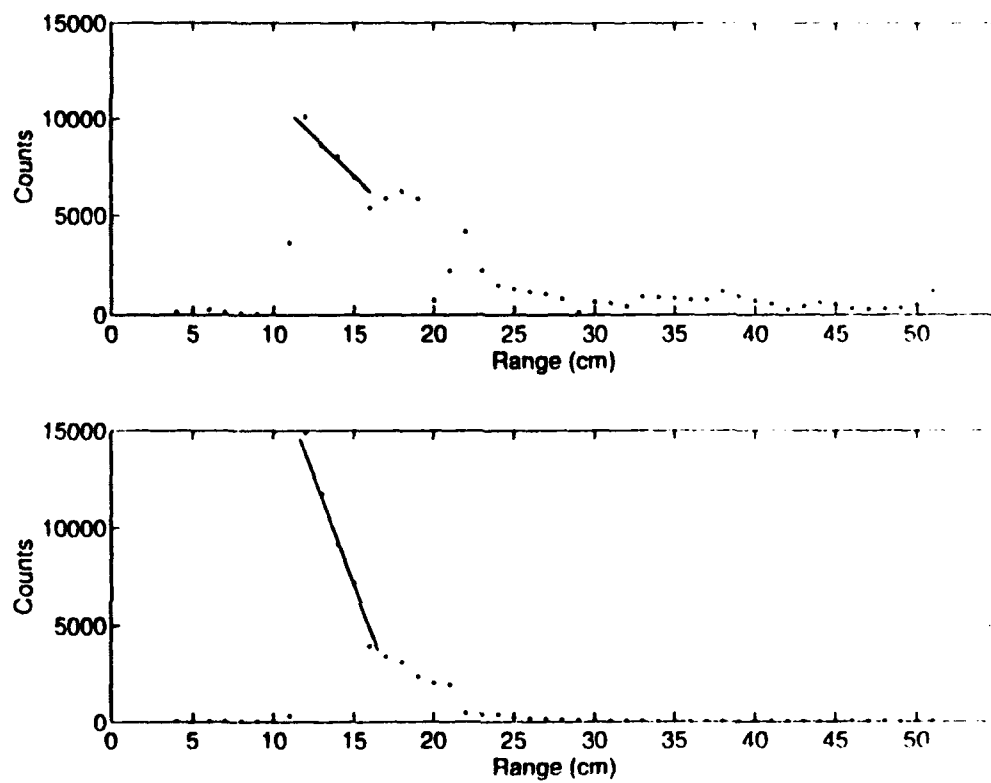
Figure 4.4 Same as Figure 4.3 but for a mass concentration of 2.1 g/l.

lines of the backscatter levels for bin 13, 14, and 15 for the 1.3 MHz and 5.2 MHz transducer have been drawn in. The backscatter level of range bin 12, the first range bin inside the mixing vessel, fits the regression line generally well for the 5.2 MHz transducer while the bin 12 backscatter level for the 1.3 MHz transducer is seen to be well above the extrapolated value from the regression line.

As previously discussed in Section III C 2, these larger then expected backscatter levels may be attributed to scatter by the plastic film window or multiple backscatter from the transducer beam side lobes coming into contact with the mixing vessel window supporting structure. To minimize the influence of this multiple backscatter from the mixing vessel on the analysis of the data, the bin 12 backscatter level for the 1.3 MHz transducer bin was extrapolated from the regression for each run. The bin 12 backscatter level for the 0 gram, mixing run was considered the baseline backscatter value and was subtracted from the backscatter level for each subsequent run . The bin 12 backscatter levels for the 5.2 MHz transducer did not require correction and were analyzed as measured.

Table 7 lists the cumulative mass, cumulative mass concentration, the data archive file, and the mean digital counts of the backscatter amplitudes for both frequencies. The backscatter levels for the 1.3 MHz transducer have been corrected as described above.

47

TABLE 7 BROAD SPECTRUM SUSPENDED SEDIMENT DATA

Cum.Mass (g)	Cum. Conc. (g/l)	CASPTS	1.3 MHz (counts)	5.2 MHz (counts)
0	0	55	-29±0	-151±26
0	0	56	0	0
0.5	0.03	57	59±18	1704±204
1.0	0.65	62	979±39	2409±265
1.5	0.10	66	1307±54	2991±239
2.0	0.13	67	1613±58	3534±318
3.0	0.19	68	2066±99	4293±343
4.0	0.26	69	2604±120	5034±403
6.0	0.39	58	3270±177	6279±565
8.0	0.52	59	3968±238	7329±660
12.0	0.78	60	5109±511	9139±731
16.0	1.0	61	9753±858	10294±926
24.0	1.6	63	7522±617	13000±1170
32.0	2.1	64	8737±664	14712±1030

Figure 4.5 shows the plot of the dependence of the backscatter levels of the suspended sediment from Monterey Wharf to the cumulative concentration. From Equation (2.9), the backscatter levels are proportional to the square root of the mass concentration. One would expect a linear relationship to arise from the square of the backscatter levels as a function of the mass concentration. Figure 4.6 shows the plot of the square of the backscatter levels for each cumulative concentration. Ignoring the obvious outlier of the 1.3 MHz backscatter
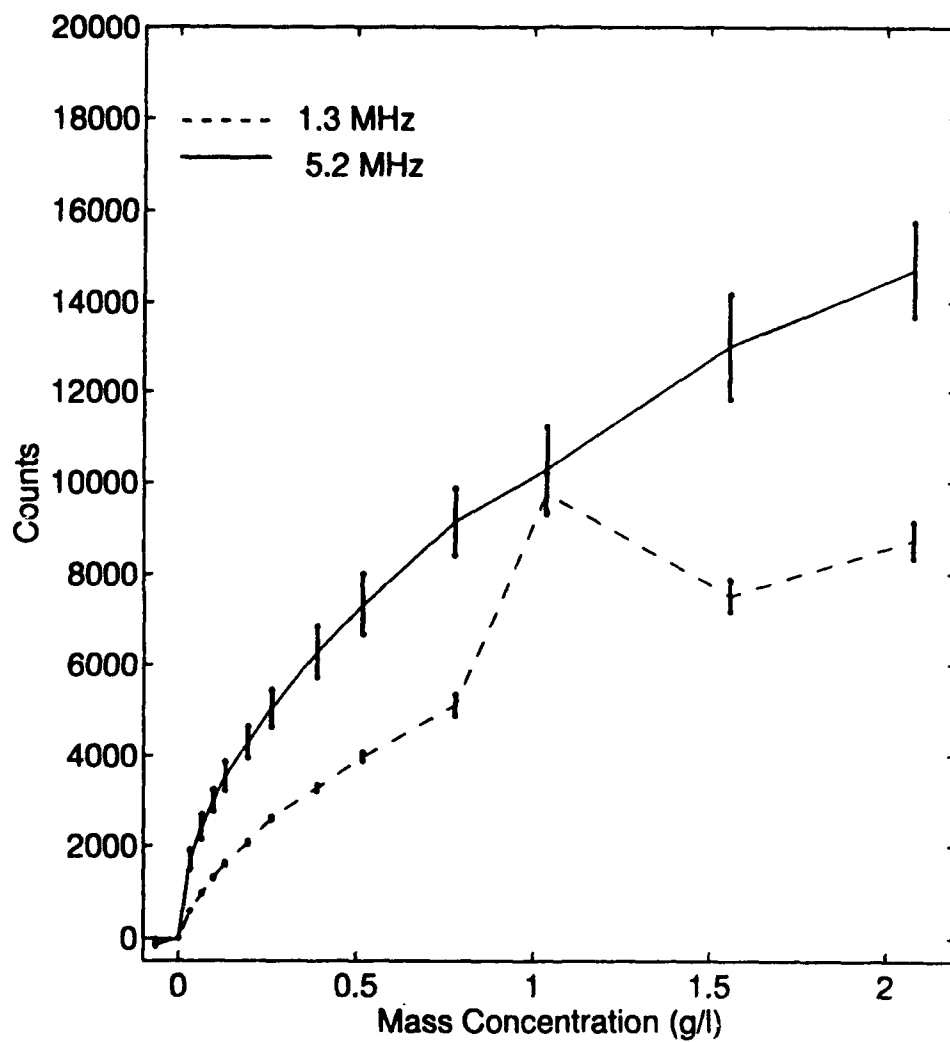
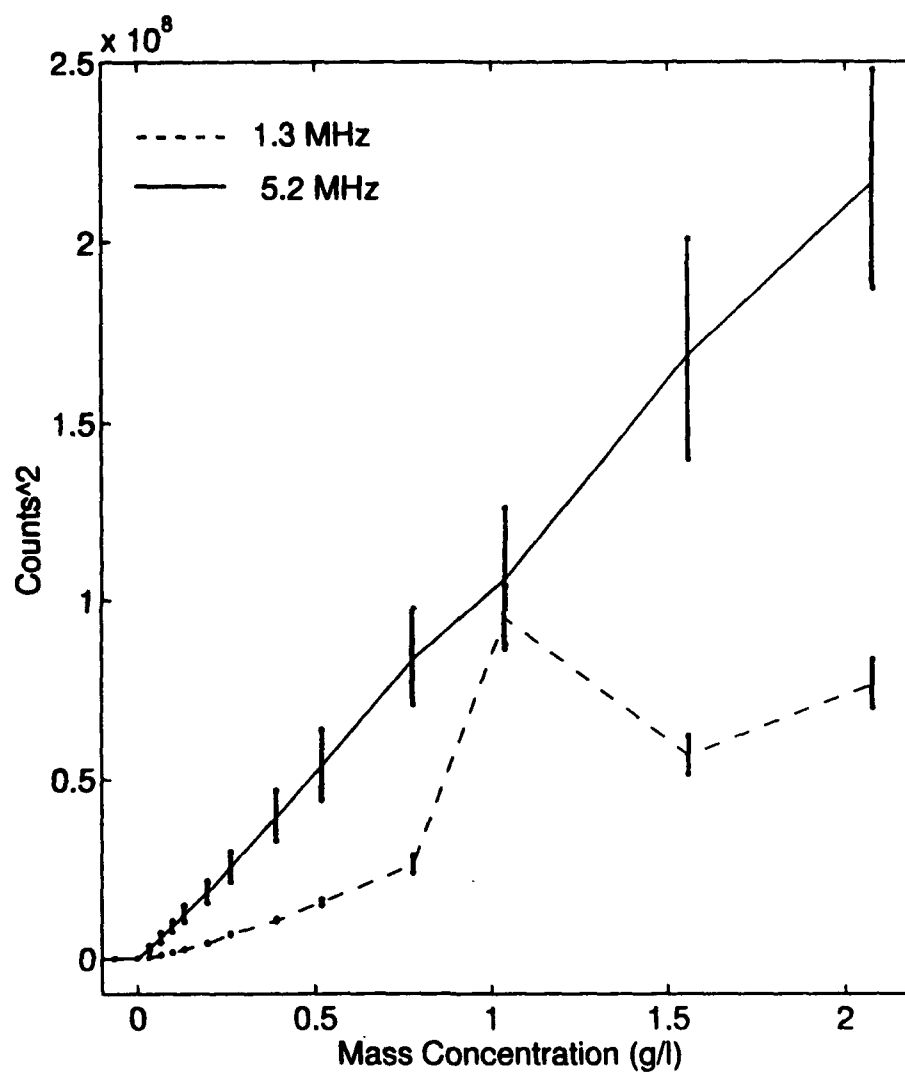Figure 4.5 Plot of the backscatter levels as a function of mass concentration.

Figure 4.6 Plot of the square of the backscatter levels as a function of mass concentration. The linear nature of the form verifies the square root proportionality between backscatter and mass concentration.

for the 1.0 g/l mass concentration, believed to be caused by a system malfunction, Figure 4.6 does indeed verify this linear relationship within the standard deviations of the backscatter counts for each mass concentration. This satisfying result emphasizes the reliability of the equipment and procedures used in this part of the study.

The slope of the regression lines discussed above represents the decrease in backscatter level with distance, or attenuation, for each sample concentration. In this case, it specifically represents the attenuation over the length of one range bin (1.68 cm) for the CASP. Table 8 lists the attenuation for each cumulative concentration and frequency. Figure 4.7 plots attenuation *versus* concentration values which can be used in field measurements to estimate the attenuation along each beam in the presence of sediment. Starting at range bin 1, the mass concentration can be estimated using Equation (2.11), then the local attenuation can be estimated from a lookup table of the form of Table 8 (again, the attenuation for the 1.3 MHz, 1 g/l mass concentration should be ignored). The backscatter level for the subsequent bins can therefore have the effects of attenuation removed.
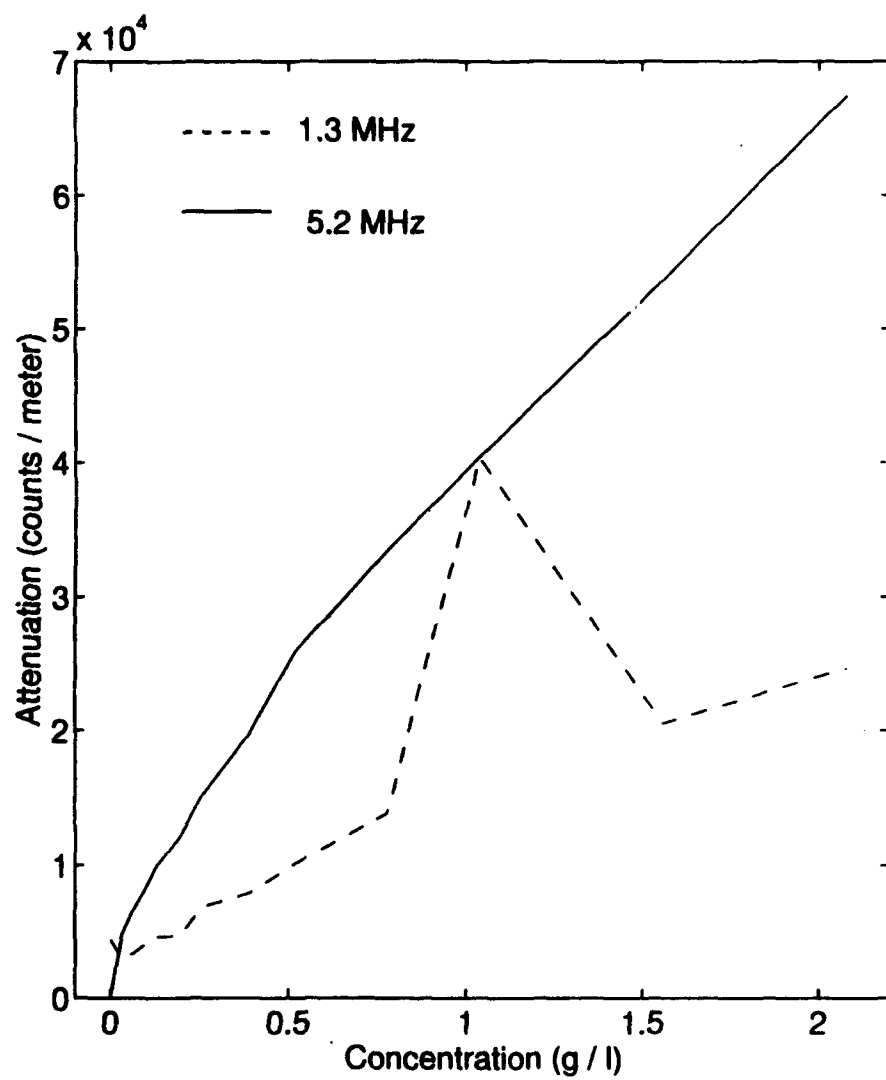
Figure 4.7 Attenuation as a function of mass concentration.

TABLE 8 ATTENUATION FOR EACH CUMULATIVE CONCENTRATION

Mass Concentration (g/l)	1.3 MHz (10^3 counts/m)	5.2 MHz (10^3 counts/m)
0	-4.38	-.00324
0.03	-2.97	-4.76
0.65	-3.41	-6.71
0.10	-4.06	-8.24
0.13	-4.62	-9.97
0.19	-4.71	-12.1
0.26	-6.91	-15.3
0.39	-7.91	-19.7
0.52	-10.1	-25.8
0.78	-13.8	-33.5
1.0	-40.4	-40.41
1.6	-20.5	-53.7
2.1	-24.6	-67.5

As the wire sensitivity calibrations have unresolved problems for the 1.3 MHz transducer, the direct measurements of backscatter *versus* a known sediment concentration shown in Table 7 and Figure 4.5 can be used to estimate the sensitivities S_1 and S_5. Following Equation (2.11), the sensitivity can be expressed as

$$S_j = \sqrt{\frac{\rho_s}{2 M_j}} \frac{K_{c_j}}{F(X, q_a)} \tag{4.1}$$

for each concentration, j, as all these variables are known. For concentrations well above
the calibration tank noise, and by rejecting the clear outlier for the 1.3 MHz transducer at the
mass concentration of 1.0 g/l, the sensitivities in Table 9 are obtained.

TABLE 9 SENSITIVITIES FOR EACH CASP TRANSDUCER CALCULATED FROM
MONTEREY WHARF SEDIMENT PARAMETERS

Cumulative Concentration (g/l)	Sensitivity (counts)			
	1.3 MHz	5.2 MHz A	5.2 MHz B	5.2 MHz C
0.19	15208	16112	14720	16397
0.26	15726	16268	14538	16318
0.39	15423	16457	14440	16475
0.52	15701	16571	15021	16430
0.78	15948	16794	14809	16646
1.0	24840	16347	14558	16312
1.6	15956	16798	14940	16348
2	15859	16438	14585	16301
Mean±STD	15867±591	16421±237	14698±177	16475±218

Figure 4.8 shows the plot of the values of the sensitivities, calculated using Equation (4.1)
and the sediment parameters for Monterey Wharf, for the 1.3 MHz and each of the three 5.2
MHz transducers. The calibration tank noise is seen in the apparent high sensitivity values
for suspended sediment concentrations less than 0.19 g/l. The sensitivity values for the
concentrations equal or greater than 0.19 g/l indicate a high consistency throughout the
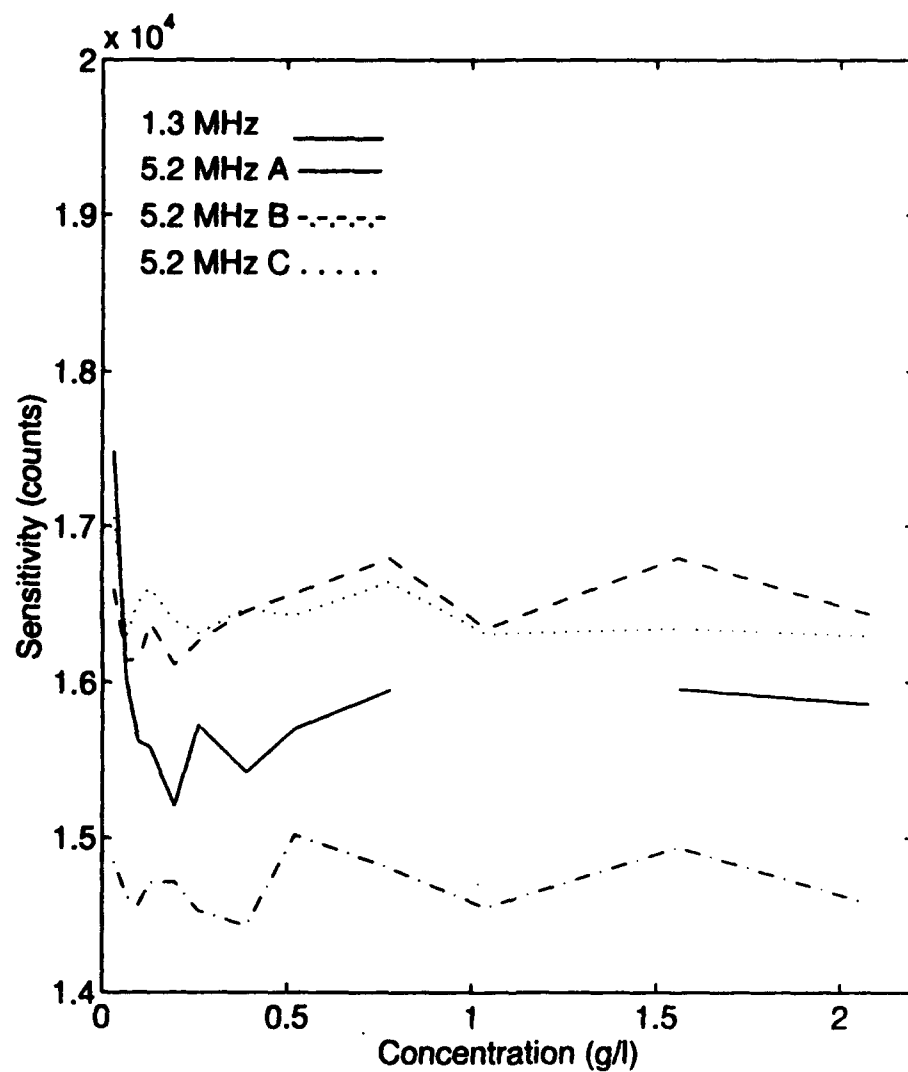range of mass concentrations for each transducer. The measured sensitivity range of the 1.3

Figure 4.8 Sensitivities for each CASP transducer calculated from parameters for sediment collected from Monterey Wharf.

MHz transducer varies 3.7%, while the sensitivities for the 5.2 MHz transducers vary only 1.4%, 1.2%, and 1.3% respectively.

Lastly, the measured sample volume defined by the transducer length and beam width is compared with the theoretical values. Table 10 lists the measured values of β_m, the angle of the first null point of the acoustic beam directivity pattern. The theoretical values calculated in Equation (2.1) were 3.1° for 1.323 MHz and 3.1° for 5.292 MHz.
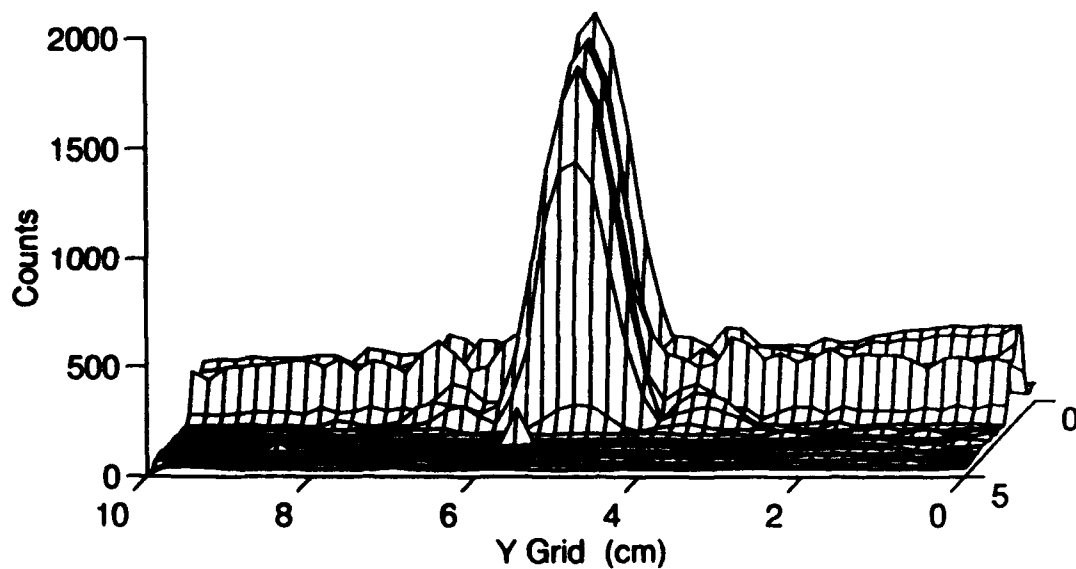
TABLE 10 β_m ANGLE OF THE FIRST NULL POINT

Frequency (MHz)	$\|\beta_m\|$ (degrees) Wire Radius (microns)				$\langle\|\beta_m\|\rangle$
	25	40	50	64	
1.323	2.04	2.66	2.66	2.66	2.51
5.292	2.86	2.86	2.86	2.65	2.81

Figures 4.9 to 4.24 show 3 D representations of the directivity pattern for the 1.3 MHz and 5.2 MHz monostatic acoustic pulse for bin 12. The X and Y plane represent the grid the CASP was moved through while backscatter data were collected. The Z axis represents the counts and the log of the square of the counts (as generated by the CASP processing program) as labeled. Also shown are end and side views of the acoustic pulse in log space.

Table 11 lists the graphically measured values of the half-power bandwidth. The theoretical value for both 1.3 and 5.2 MHz was 2.6°.
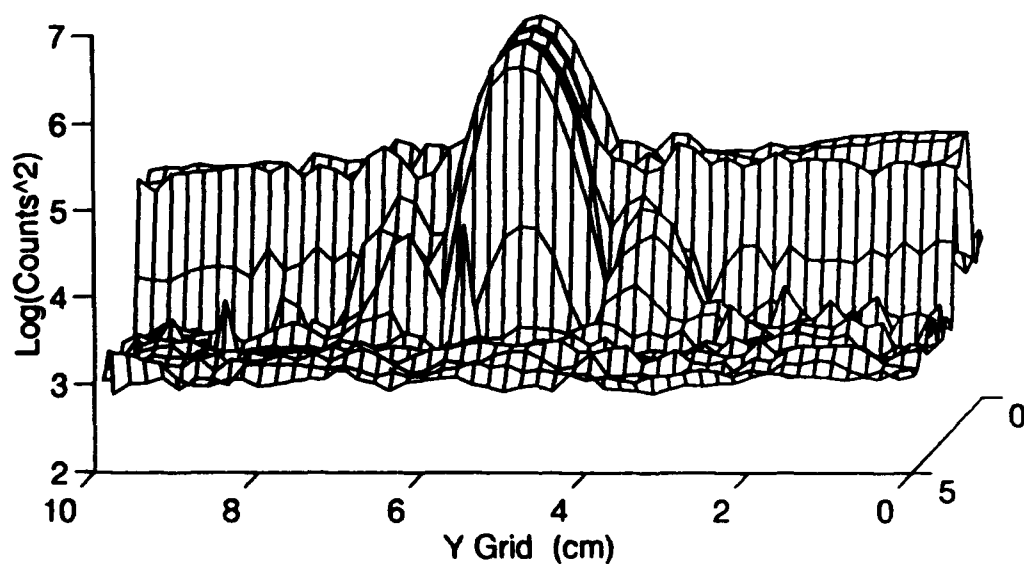
Figure 4.9 3 D representation of the monostatic acoustic pulse for 1.3 MHz and wire of radius 25 microns in log and linear space.
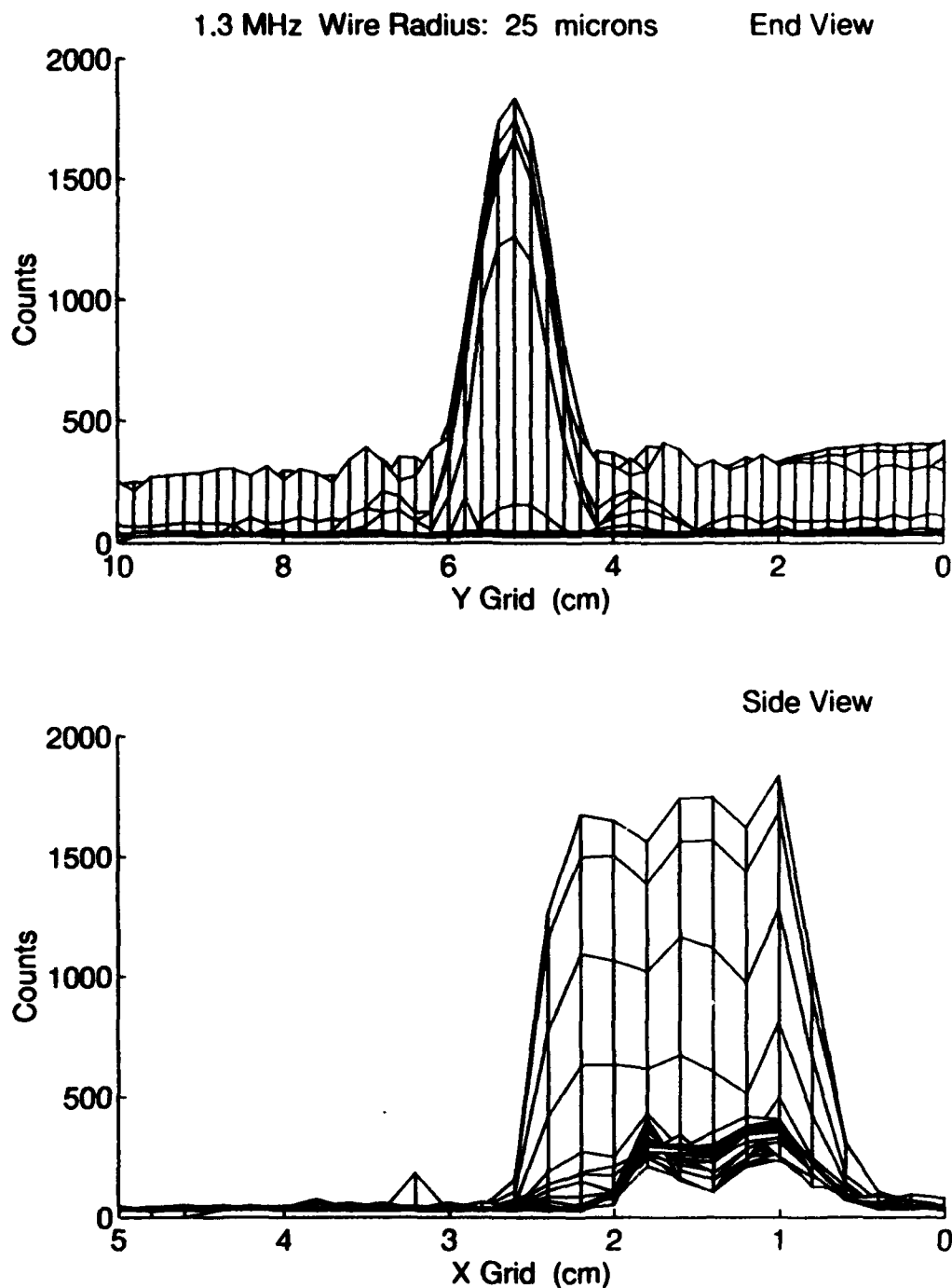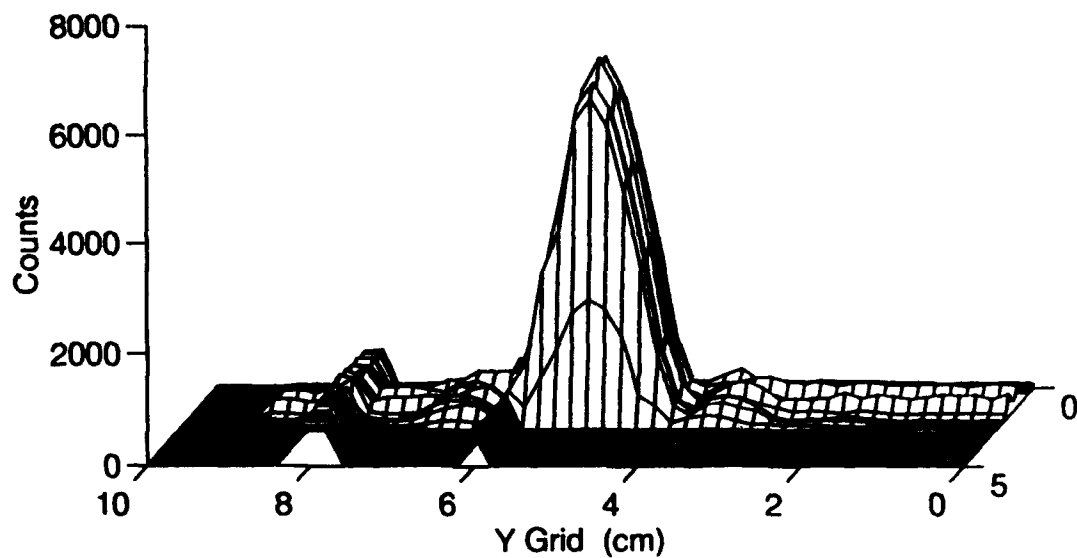
Figure 4.10 End and side views of the monostatic acoustic pulse for 1.3 MHz and wire of radius 25 microns.

1.3 MHz Wire Radius: 40 microns Linear Space

Log Space

Figure 4.11 3 D representation of the monostatic acoustic pulse for 1.3 MHz and wire of radius 40 microns in log and linear space.

59

Figure 4.12 End and side views of the monostatic acoustic pulse for 1.3 MHz and wire of radius 40 microns.

1.3 MHz Wire Radius: 50 microns   Linear Space
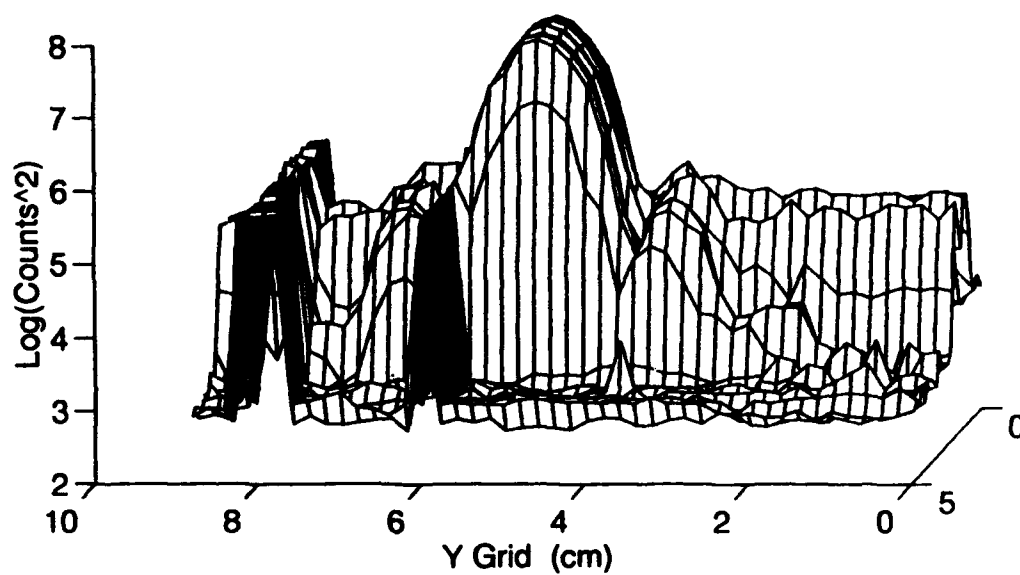
Log Space

Figure 4.13 3 D representation of the monostatic acoustic pulse for 1.3 MHz and wire of radius 50 microns in log and linear space.
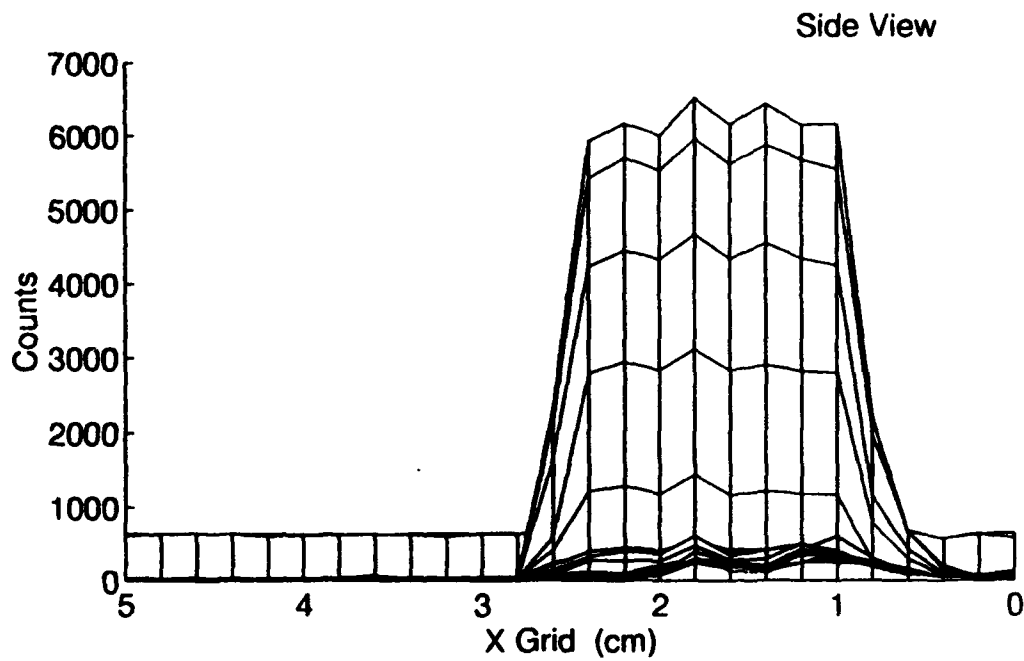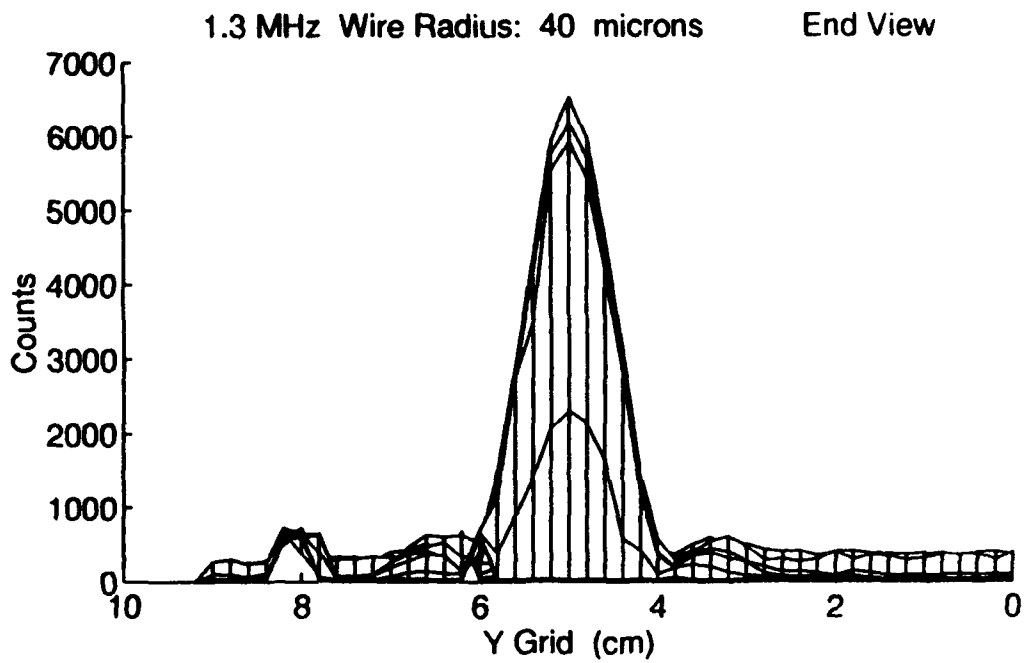
Figure 4.14. End and side views of the monostatic acoustic pulse for 1.3 MHz and wire of radius 50 microns.

1.3 MHz Wire Radius: 64 microns Linear Space

Figure 4.15 3 D representation of the monostatic acoustic pulse for 1.3 MHz and wire of radius 64 microns in log and linear space.

63

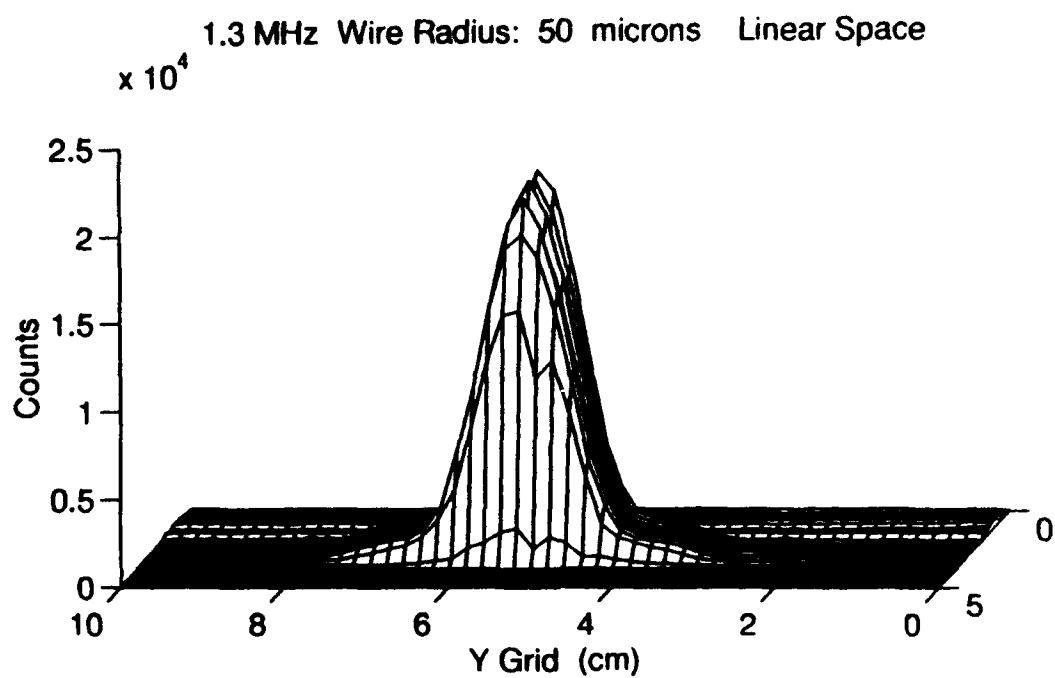**Figure 4.16.** End and side views of the monostatic acoustic pulse for 1.3 MHz and wire of radius 64 microns.

5.2 MHz Wire Radius: 25 microns Linear Space

Figure 4.17 3 D representation of the monostatic acoustic pulse for 5.2 MHz and wire of
radius 25 microns in log and linear space.

65

Figure 4.18 End and side views of the monostatic acoustic pulse for 5.2 MHz and wire of radius 25 microns.
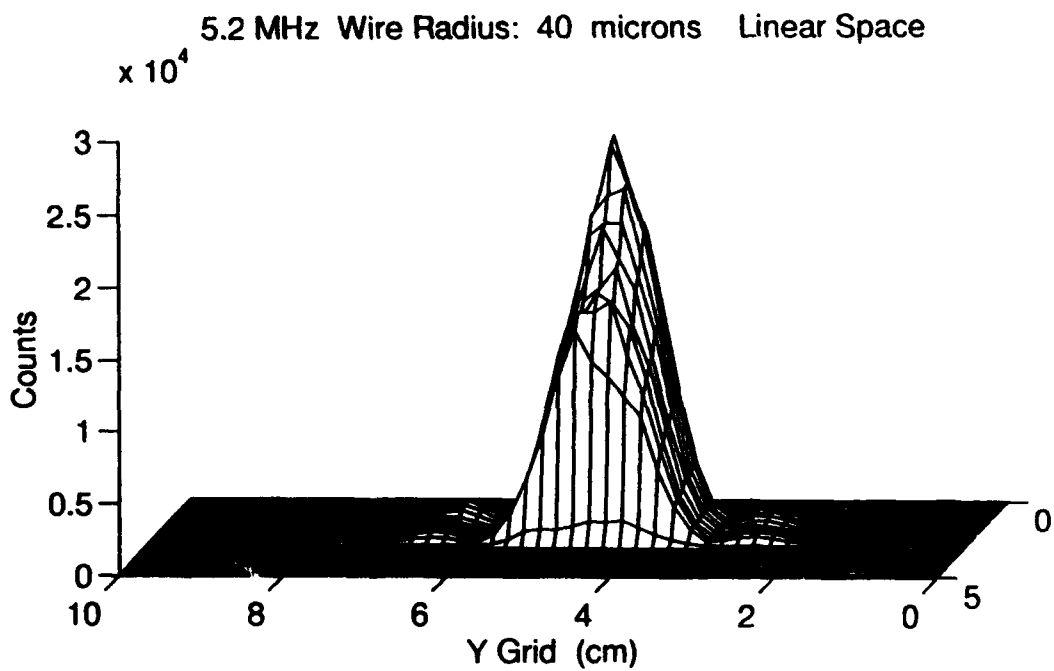
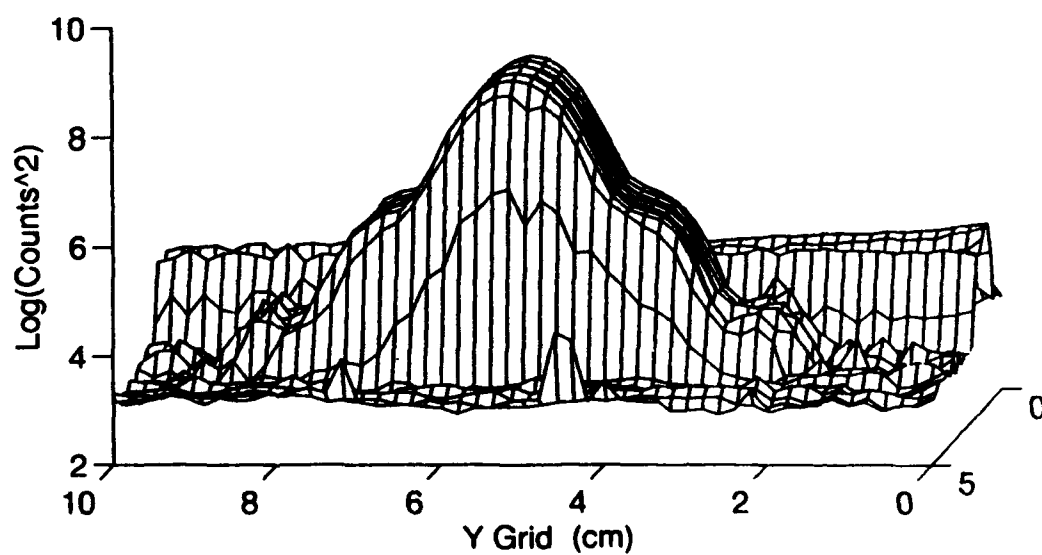5.2 MHz Wire Radius: 40 microns   Linear Space
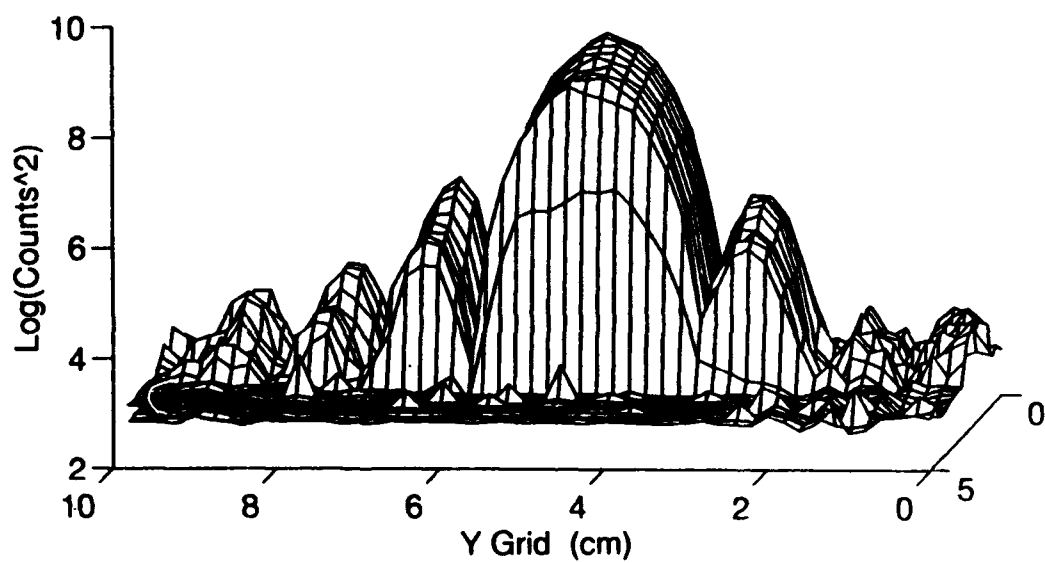
Figure 4.19 3 D representation of the monostatic acoustic pulse for 5.2 MHz and wire of radius 40 microns in log and linear space.
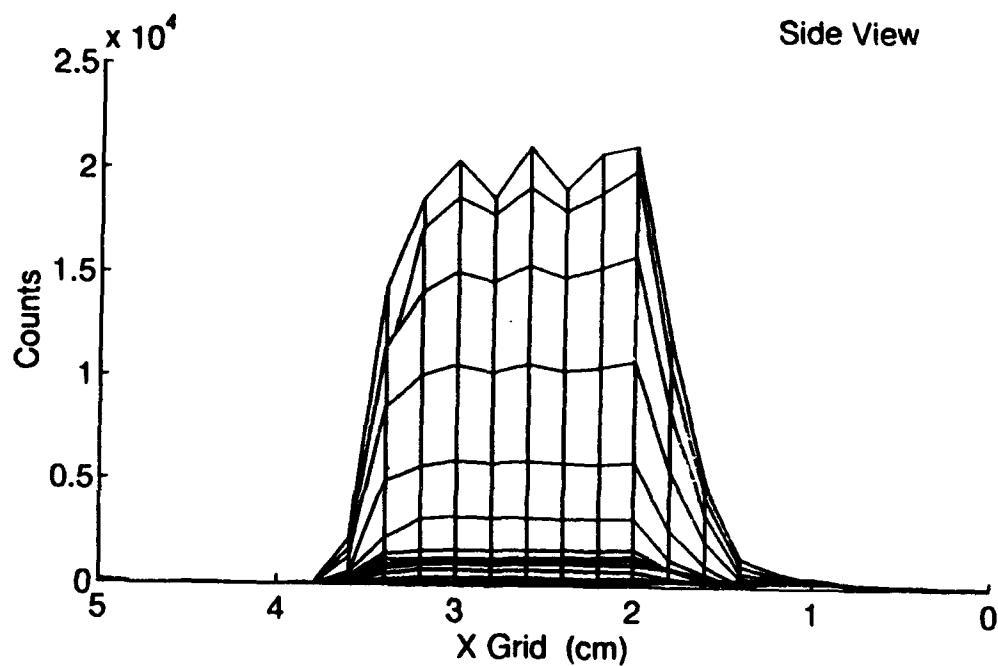
67
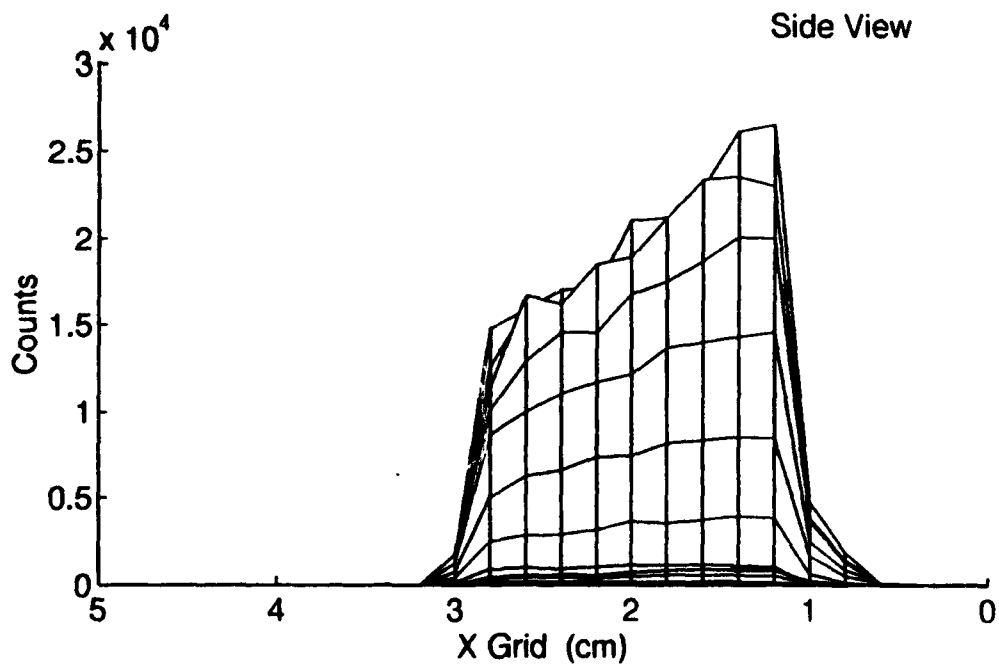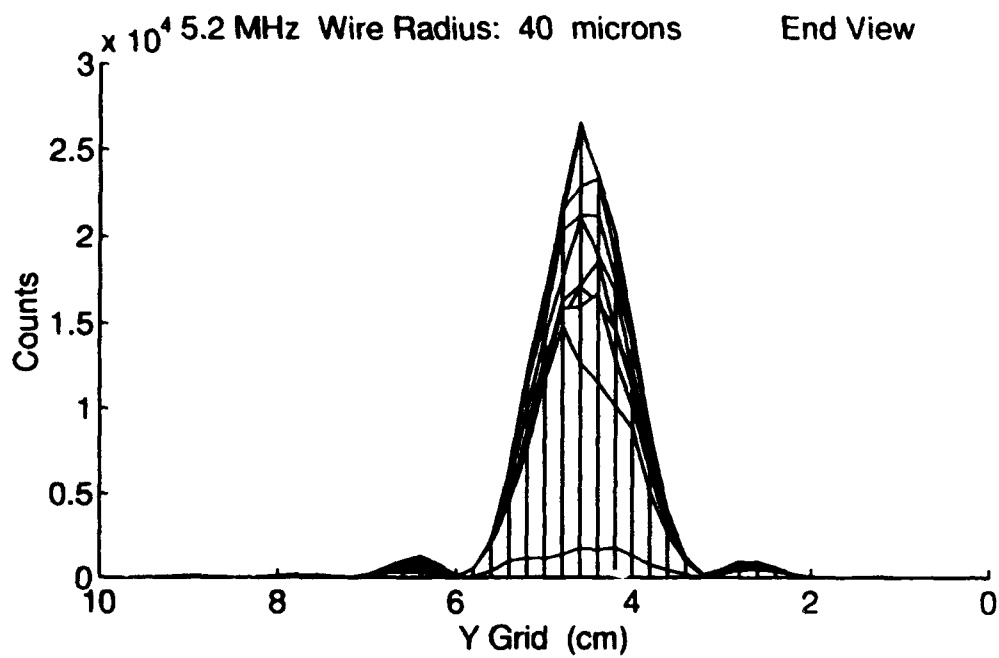
Figure 4.20 End and side views of the monostatic acoustic p.... .or 5.2 MHz and wire of radius 40 microns.
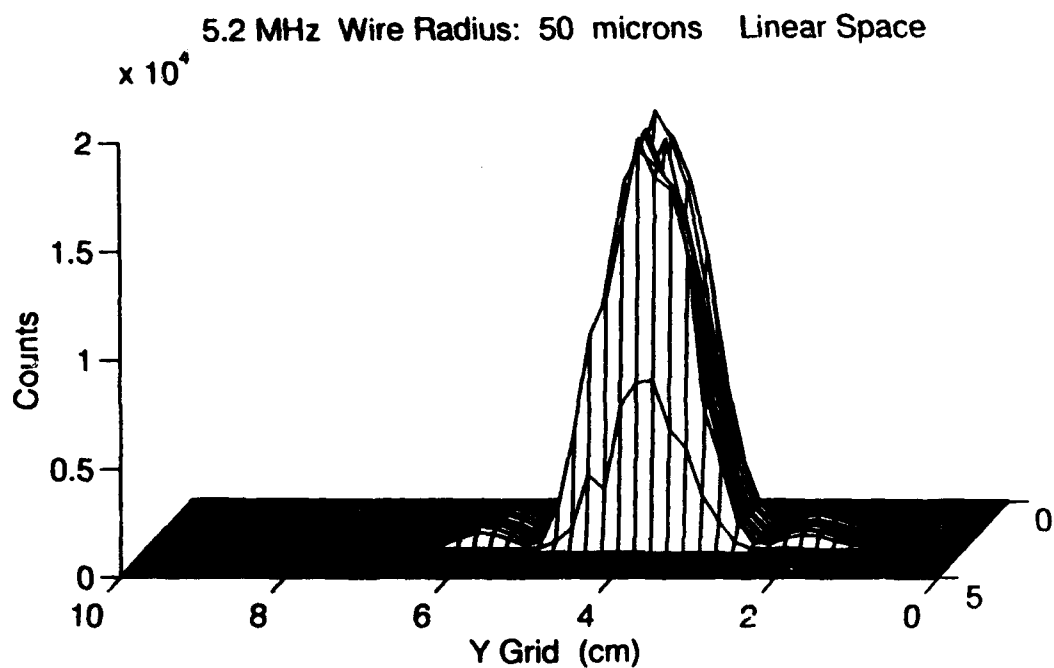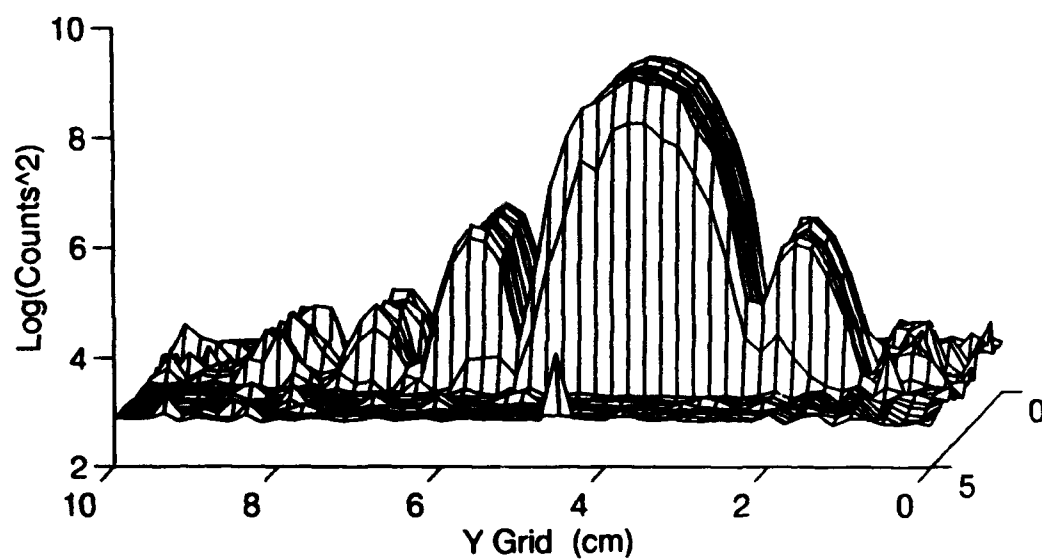
Figure 4.21 3 D representation of the monostatic acoustic pulse for 5.2 MHz and wire of radius 50 microns in log and linear space.
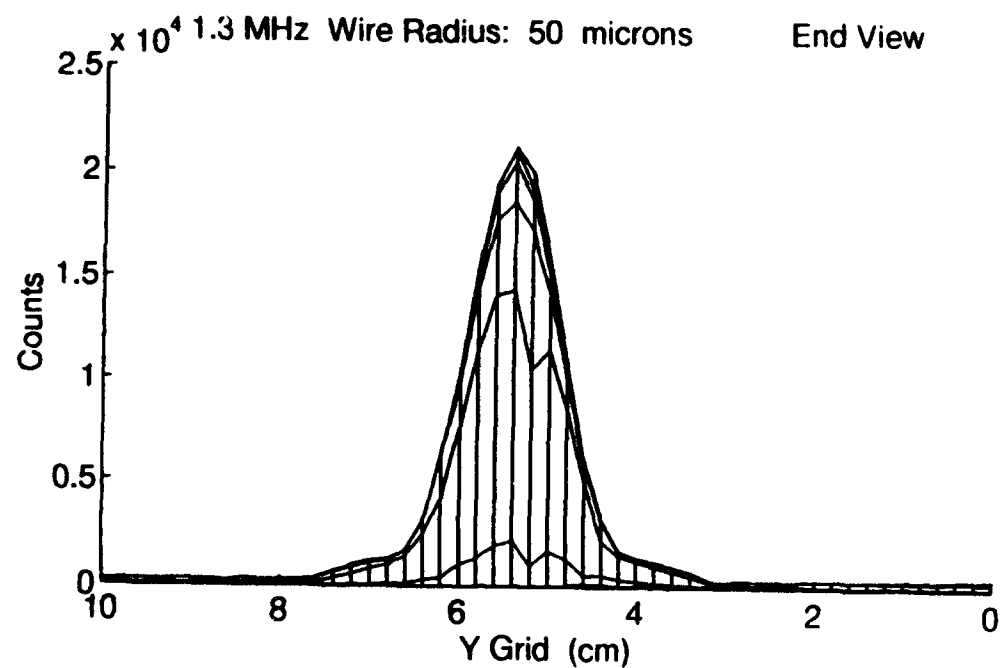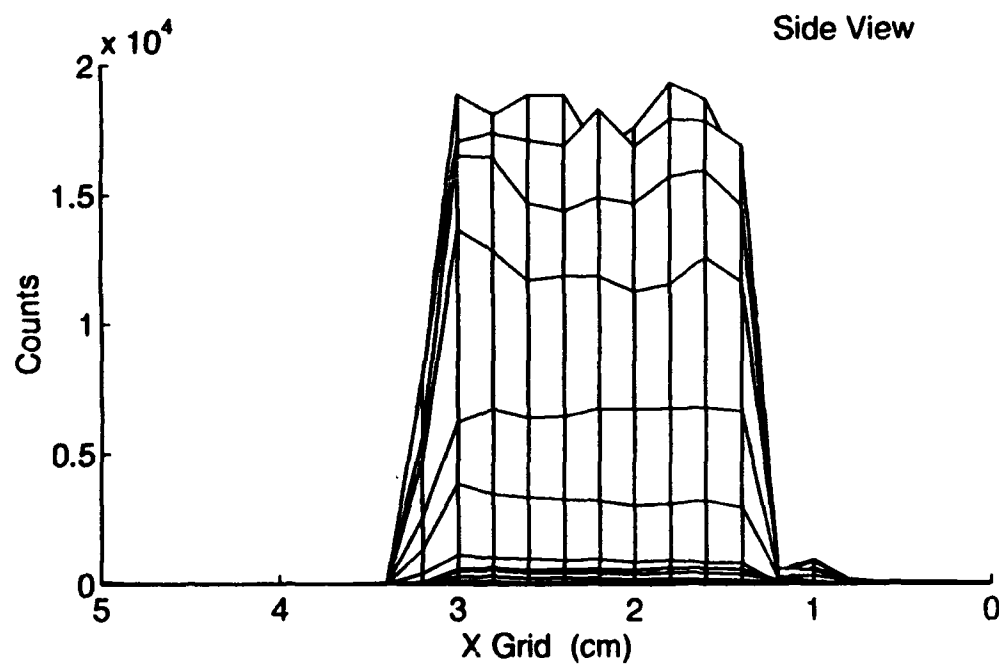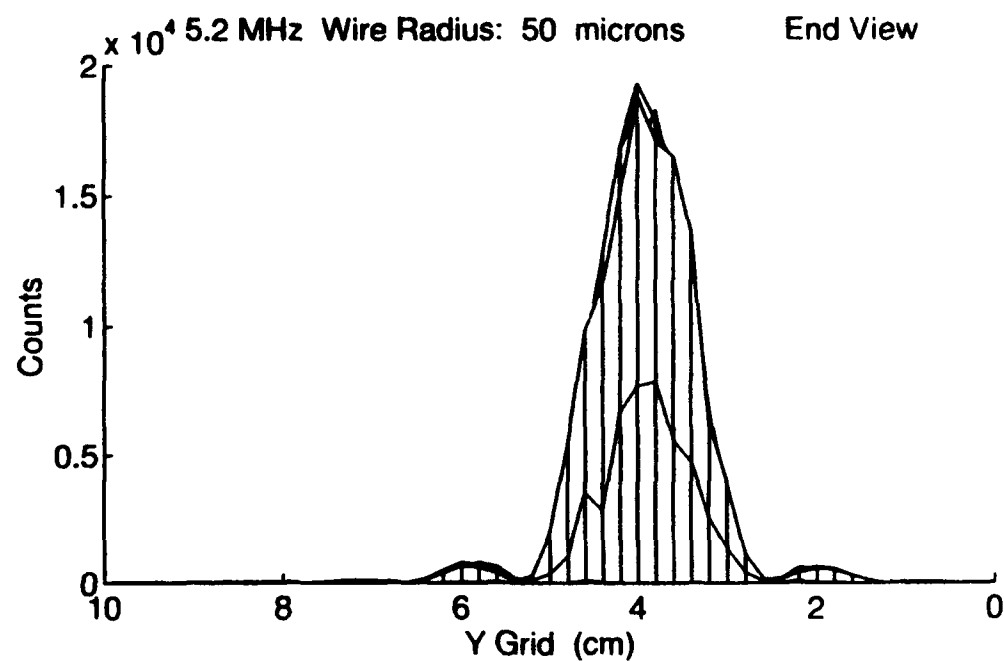
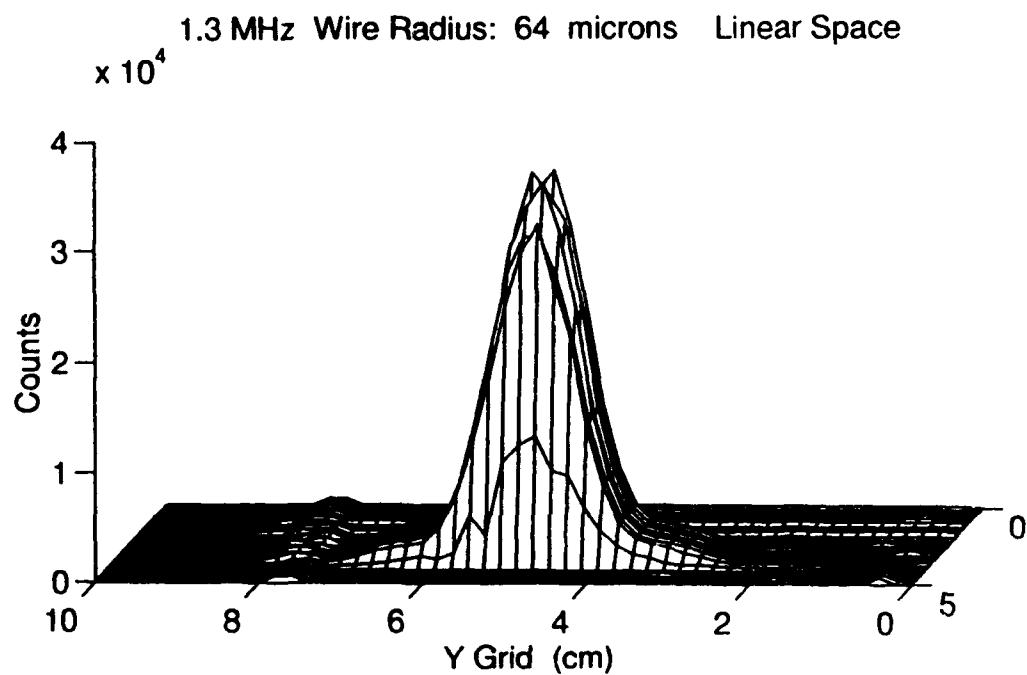Figure 4.22 End and side views of the monostatic acoustic pulse for 5.2 MHz and wire of radius 50 microns.

70

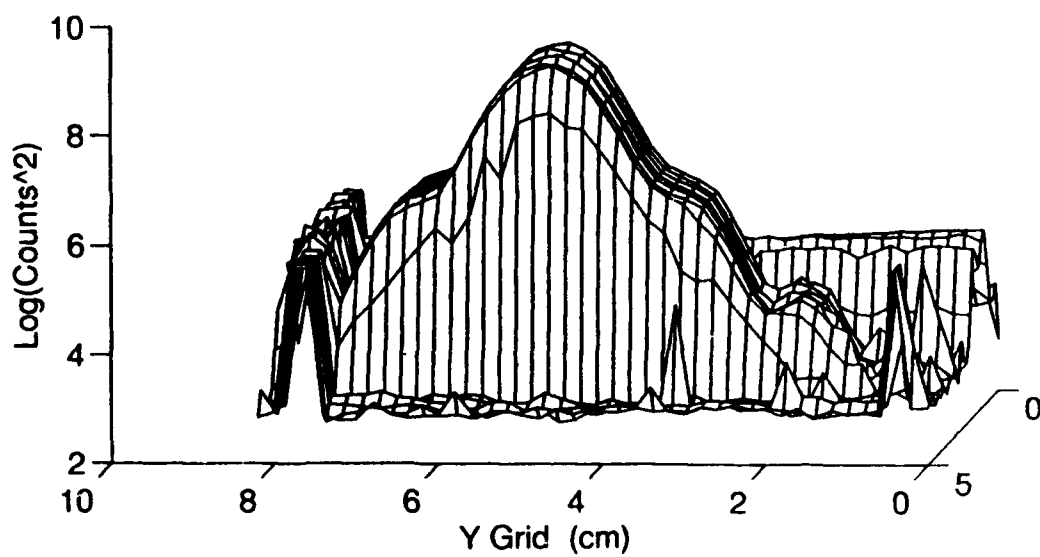5.2 MHz Wire Radius: 64 microns   Linear Space

Log Space
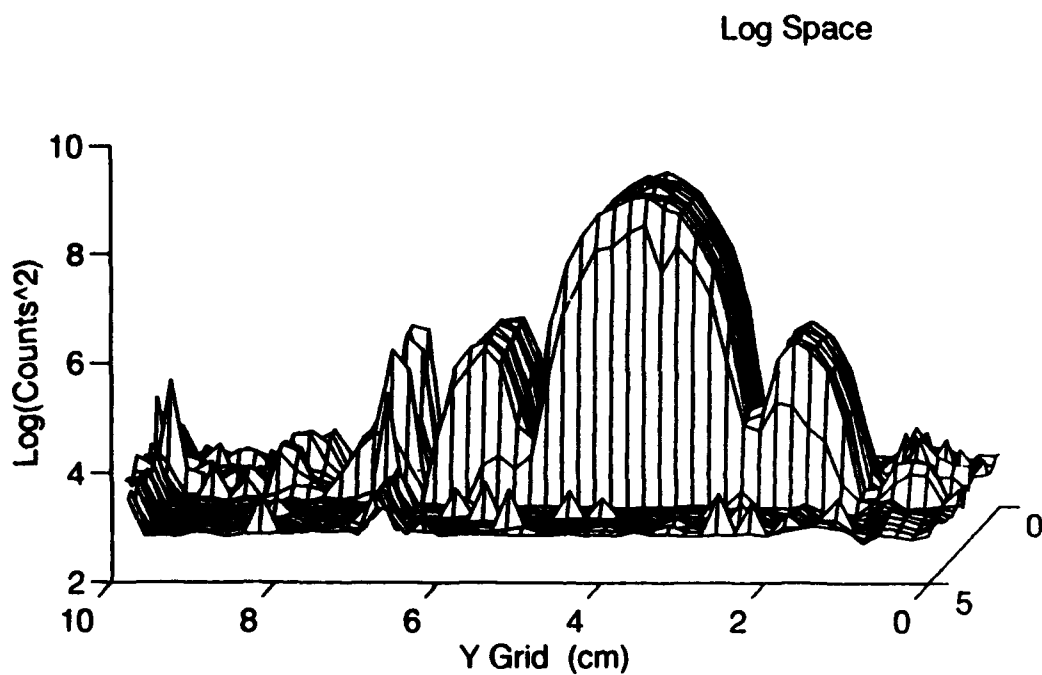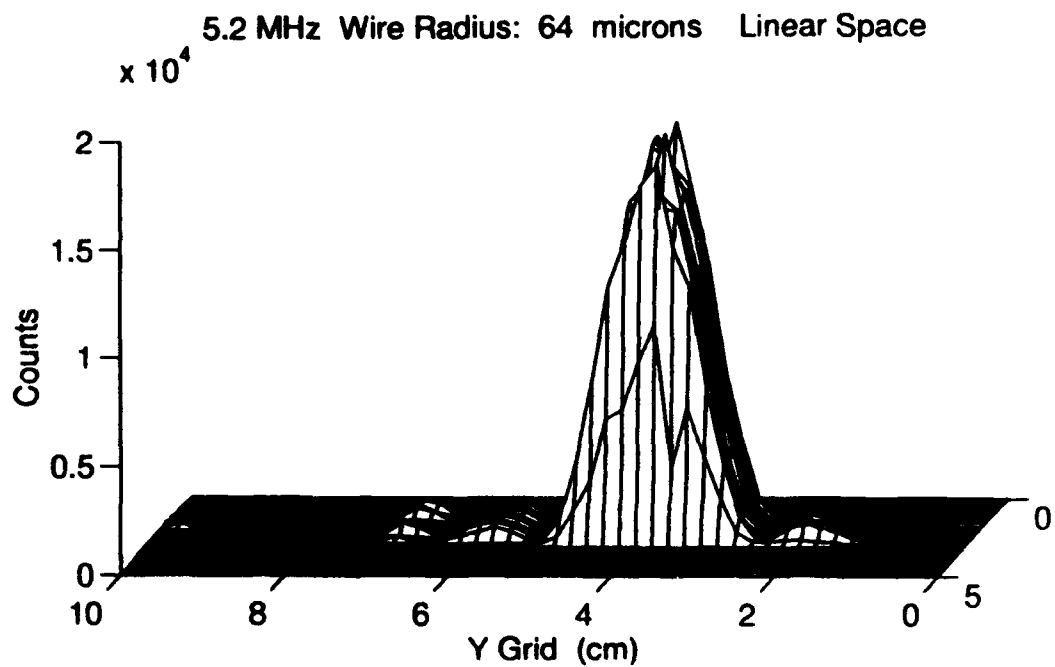
Figure 4.23 3 D representation of the monostatic acoustic pulse for 5.2 MHz and wire of radius 64 microns in log and linear space.
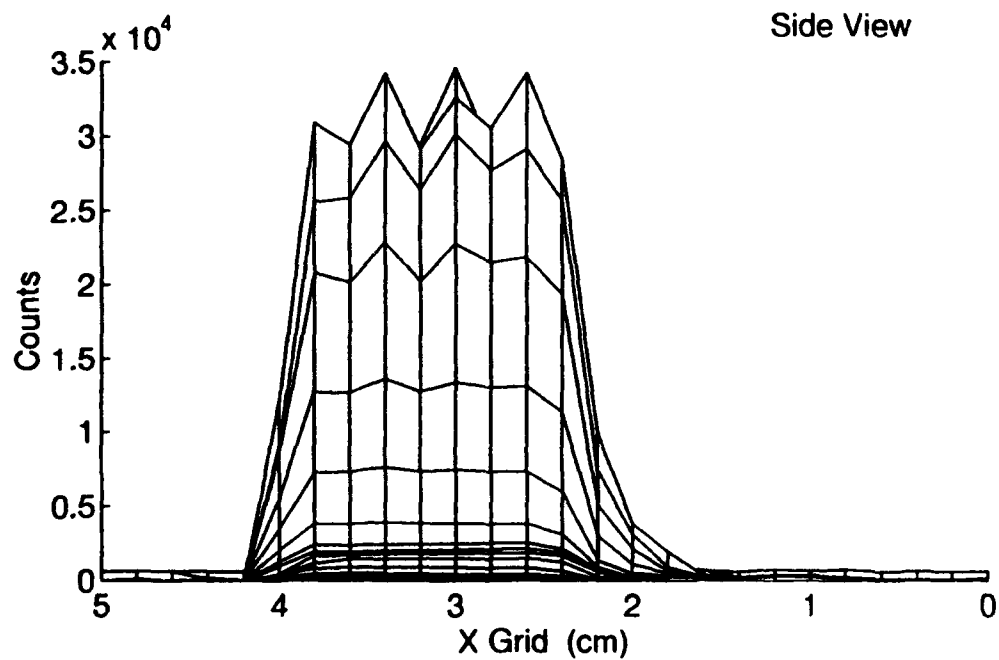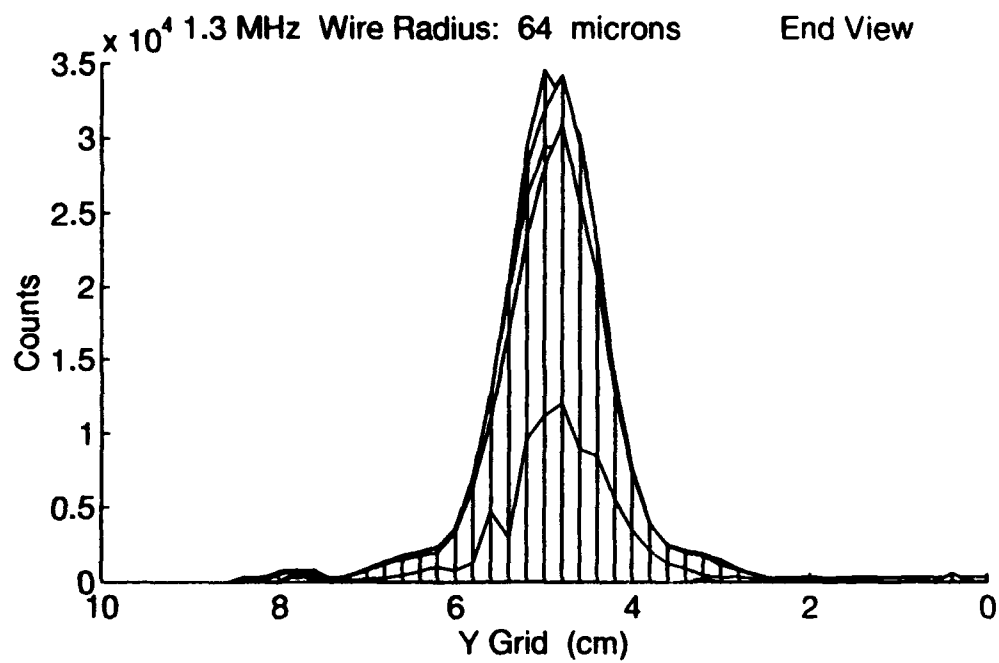
71

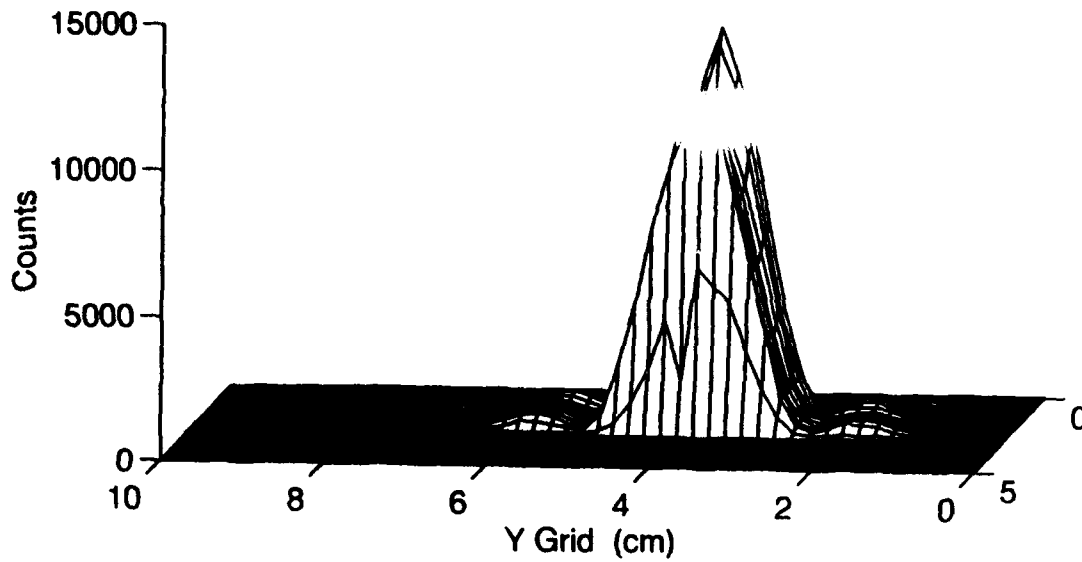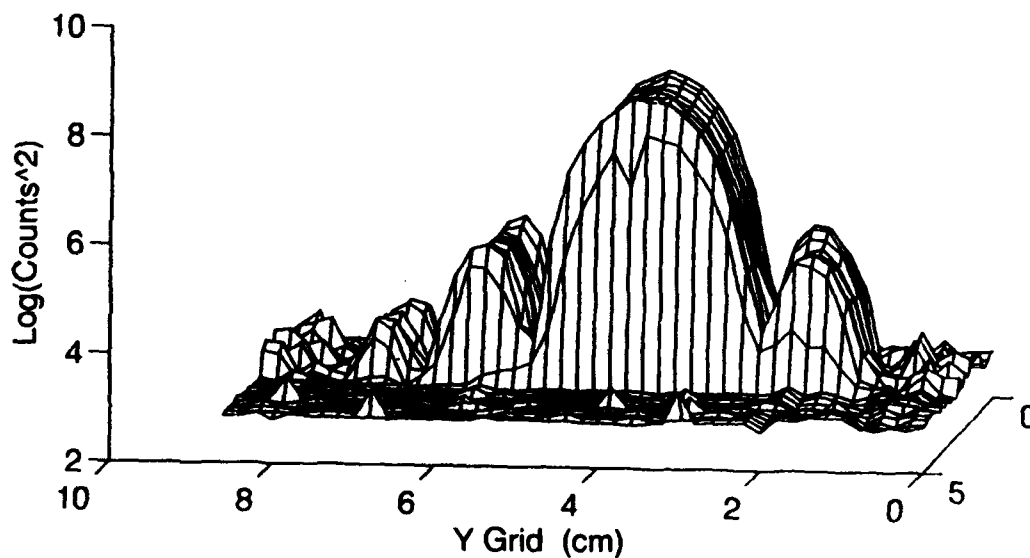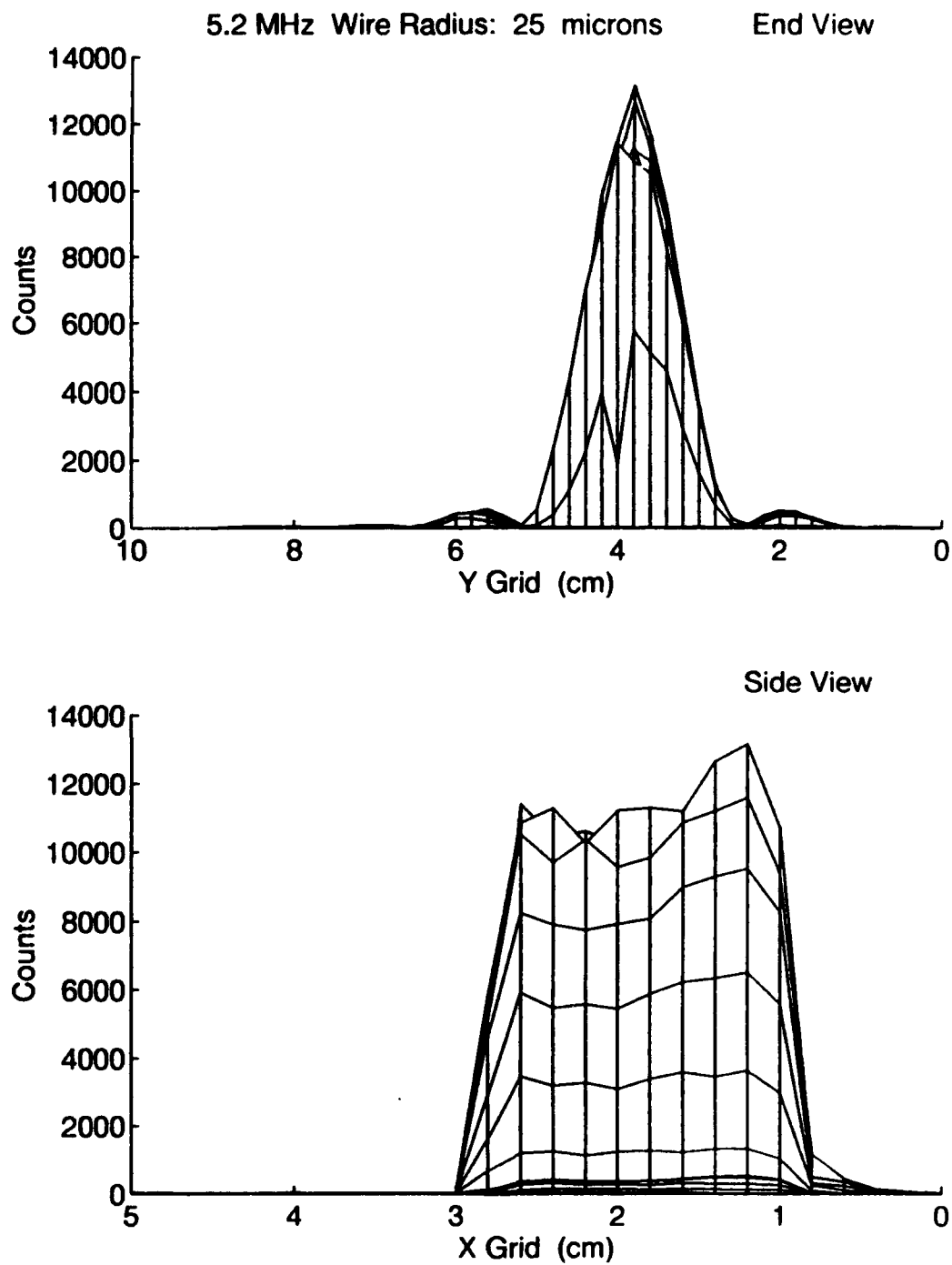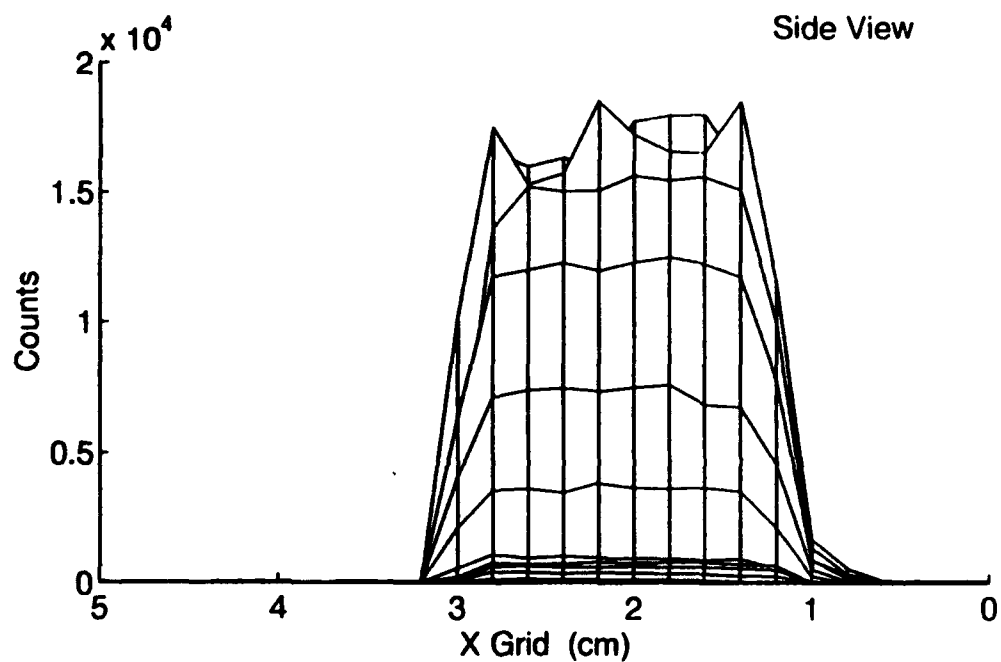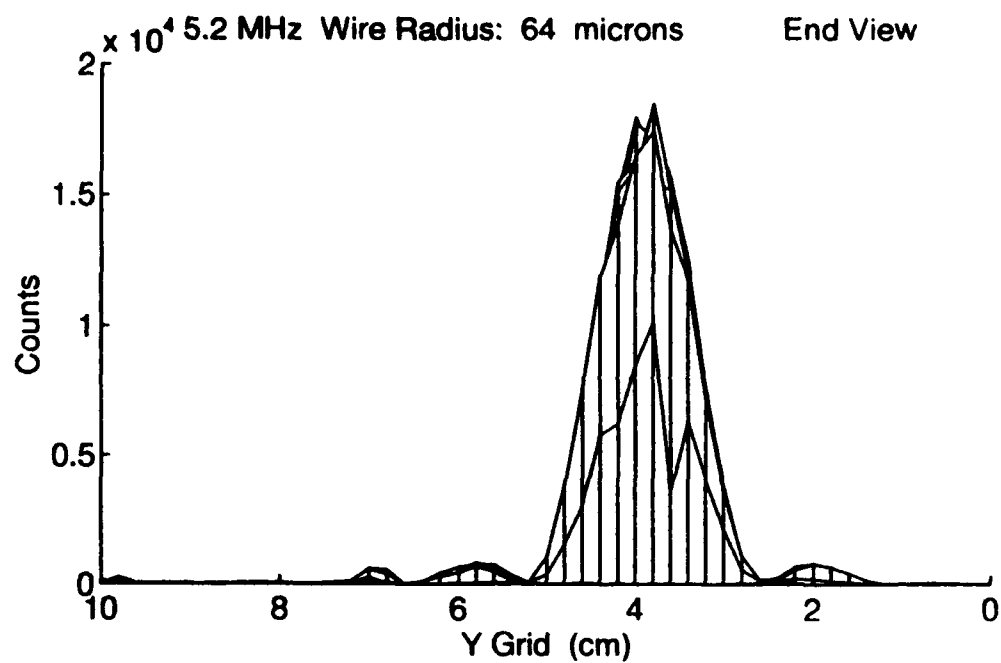Figure 4.24 End and side views of the monostatic acoustic pulse for 5.2 MHz and wire of radius 64 microns.

TABLE 11 β_0 HALF-POWER BANDWIDTH

Frequency (MHz)	$\| \beta_0 \|$ (degrees) Wire Radius (microns)				$\langle \| \beta_0 \| \rangle$
	25	40	50	64	
1.323	1.2	1.2	1.2	1.2	1.2
5.292	1.2	1.2	1.2	1.2	1.2

Comparison of the calculated values of β_m , and β_0 indicate the acoustic beam for both 1.3 MHz and 5.2 MHz are slightly narrower than calculated by theory, but show a close to ideal beam response.

Table 12 lists L_p , the length of the monostatic pulse length for both frequencies. The theoretical value is 0.0168 meters. Again, there is good agreement between the calculated and measured values suggesting that the acoustic transmitter, transducer and receiver system is performing as designed .

TABLE 12   MONOSTATIC PULSE LENGTH

Frequency (MHz)	(L_p) $(10^{-2}$ meter) Wire Radius (microns)				$\langle \| L_p \| \rangle$
	25	40	50	64	
1.323	1.7	1.7	1.7	1.6	1.7
5.292	1.9	1.7	1.9	1.9	1.9

V. CONCLUSIONS AND RECOMMENDATIONS

As discussed in Section IV A, the sensitivity for each wire should be equal for each of the frequencies being evaluated based on the dependence of the form factor on the frequency of the incident energy and the size of the fixed wire. The sensitivities calculated for the 5.2 MHz transducer, $3.30 \pm 0.70 \times 10^6$ counts, were consistent to within 21 %. The sensitivities calculated for the 1.3 MHz transducer were inconsistent with a mean value of $9.28 \pm 5.28 \times 10^6$ counts. This large variation is believed to be due to a strong angular dependence between the orientation of the fixed wire target and the 1.3 MHz transducer. While use of a fixed wire as a standard target avoids the z-axis dependence and the difficulty of locating targets of minute size in the narrow acoustic beam, these advantages appear to be outweighed by critical angular positioning requirements. The sensitivities of the two frequencies are parameters required in the estimation of both the mean particle radius and the mass concentration of the suspended sediment using the inversion method discussed in this work. The angular dependency between a fixed wire target and the 1.3 MHz transducer can be avoided by the use of a single small, spherical target such as a bead or BB, suspended in the acoustic beam. Although there will be no angular dependence between the spherical target and the transducer due to the symmetry of the target, care must be taken to accurately locate the target in the center of the very narrow acoustic beam.

The values of the sensitivities obtained from Eq. (4.1) and the known suspended sediment parameters were highly consistent for the 1.3 MHz and the three 5.2 MHz transducers indicating the equipment and procedure were highly reliable.

The proportionality between the backscatter levels and the square root of the mass concentration confirms the reliability of the experimental method for the collection of backscatter data from the suspended sediment. The cause of the single outlying point in the 1.3 MHz data is unknown, but is believed to be a system malfunction and not indicative of the technique or noise performance.

The form of the curves for the theoretical ratio of $F(X_9, \sigma_g)/F(X_1, \sigma_g)$, shown in Figure 2.6, shows a low sensitivity to the choice of σ_g, and sufficient slope to allow a satisfactory estimation of the mean particle radius of the lognormal sediment population over a range from 20 to 100 microns using the two-frequency inversion method described here. The slope of the curves approaches zero for radii greater than 100 microns (200 micron diameter), seriously reducing the ability of the $F(X_5, \sigma_g)/F(X_1, \sigma_g)$ ratio to discriminate mean radius sizes outside this range.

The reflective material of the test tank results in the constructive reflection of a portion of the acoustic energy off the sides and bottom of the tank. This creates regions of ambiguous backscatter amplitudes which can be misinterpreted as the backscatter from a test target or suspended sediment under investigation. Additional analysis of these "range" ambiguities is required to identify their location to avoid positioning of test targets or the mixing vessel near these positions. This becomes particularly critical for low concentrations and other weak targets.

75

Calibration runs using sediment samples with different lognormal distribution parameters will add to the verification of the inversion method by use of the different $F(X_s, \sigma_g)/F(X_1, \sigma_g)$ curves determined by the value of σ_g. Furthermore, the attenuation *versus* concentration characteristics for different sediment types will be applied in along-beam mass estimates to compensate for along-beam attenuation in the backscatter levels, and could possibly provide additional discrimination of sediment types.

The two minute duration of the suspended sediment runs was chosen to allow the collection of a sufficient amount of data to ensure the effect of statistical noise was minimized. Further investigation of the temporal resolution of this inversion technique will reveal the minimum sampling time required to arrive at a satisfactory and consistent estimation of sediment particle size distribution and mass concentration.

This study represents the first stage of characterizing the backscatter amplitude performance of the CASP, and implements a technique to estimate mean particle size and sediment mass concentration. While the wire target backscatter sensitivity calibrations were not fully successful, the sample volume characteristics were successfully compared with theoretical values. Baseline performance data have been measured for a typical sediment population over a wide range of concentrations, enabling the system sensitivities to be estimated.

APPENDIX A

SEDIMENT SIZE DISTRIBUTION REPORT

Project	CASP	Project #	93L
Sample I.D.	3-1Monterey Wharf	Lab Number	0
Sample Date	9/29/93	Analysis Date	10/1 R\9 3

	size ranges			
	phi	mm	Fract. %	Cum. %
Gravel	<0	>1.0	18.07	18.07
Coarse Sand	1	0.500	14.36	32.43
Medium/Fine Sand	4	0.063	66.09	98.52
Coarse Silt	5	0.031	1.48	100.00
Medium/Fine Silt	>5	<.031	0.00	100.00

excluded from analysis
% Debris 0.0
Debris Type 0.001

mm	Phi	Cum. %	Fract. %
4.0000	-2.0	0.0	0.0
2.0000	-1.0	10.5	10.5
1.0000	0.0	18.1	7.5
0.5000	1.0	32.4	14.4
0.2500	2.0	60.0	27.6
0.1250	3.0	97.1	37.1
0.0625	4.0	98.5	1.1
0.0313	5.0	100.0	1.5
0.0078	7.0	100.0	0.0

Grain Size Statistics (Folk & Ward)

	mm	phi
Mean	0.421	1.25
Median	0.296	1.75
Sorting	0.451	1.15
Skewness		-0.61
Kurtosis		0.93

77
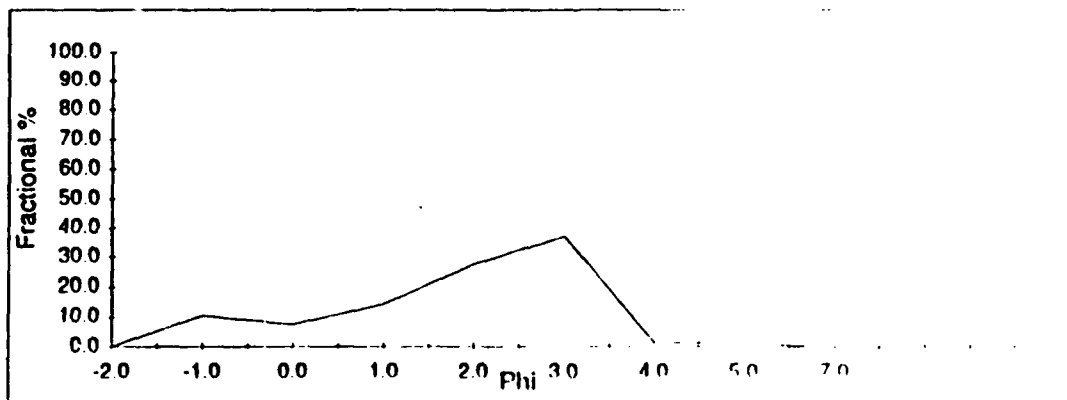
Project	CASP		Project #		9 3l.
Sample I.D.	3-2Monterey Wharf		Lab Number		0
Sample Date	9/29/93		Analysis Date		10/13/93

	size ranges			
	phi	mm	Fract. %	Cum. %
Gravel	<0	>1.0	22.11	22.11
Coarse Sand	1	0.500	16.21	38.32
Medium/Fine Sand	4	0.063	60.11	98.43
Coarse Silt	5	0.031	1.57	100.00
Medium/Fine Silt	>5	<.031	0.00	100.00

excluded from analysis
% Debris 0.0
Debris Type 0.001

	mm	Phi	Cum. %	Fract. %
	4.0000	-2.0	0.0	0.0
	2.0000	-1.0	13.9	13.9
Grain Size Statistics (Folk & Ward)	1.0000	0.0	22.1	8.2
	0.5000	1.0	38.3	16.2

	mm	phi	0.2500	2.0	62.0	23.7
Mean	0.482	1.05	0.2500	2.0	62.0	23.7
Median	0.327	1.61	0.1250	3.0	95.7	33.7
Sorting	0.404	1.31	0.0625	4.0	98.4	2.7
Skewness		-0.51	0.0313	5.0	100.0	1.6
Kurtosis		0.80	0.0078	7.0	100.0	0.0

Project	CASP		Project #	93L
Sample I.D.	3-3Monterey Wharf		Lab Number	0
Sample Date	9/29/93		Analysis Date	10/13/93

	size ranges			
	phi	mm	Fract. %	Cum %
Gravel	<0	>1.0	17.86	17.86
Coarse Sand	1	0.500	11.55	32.11
Medium/Fine Sand	4	0.063	66.07	98.48
Coarse Silt	5	0.031	1.52	100.00
Medium/Fine Silt	>5	<.031	0.00	100.00

excluded from analysis
% Debris 0.0
Debris Type 0.001

			mm	Phi	Cum. %	Fract. %
			4.0000	-2.0	0.0	0.0
			2.0000	-1.0	11.0	11.0
Grain Size Statistics (Folk & Ward)			1.0000	0.0	17.9	6.9
	mm	phi	0.5000	1.0	32.4	14.6
Mean	0.423	1.24	0.2500	2.0	60.6	28.2
Median	0.298	1.75	0.1250	3.0	97.5	36.9
Sorting	0.452	1.14	0.0625	4.0	98.5	1.0
Skewness		-0.62	0.0313	5.0	100.0	1.5
Kurtosis		0.93	0.0078	7.0	100.0	0.0

Project	CASP		Project #	93L.
Sample I.D.	1-1Asilomar		Lah Number	0
Sample Date	9/29/93		Analysis Date	10\13\93

		size ranges			
		phi	mm	Fract. %	Cum. %
Gravel		<0	>1.0	17.78	17.78
Coarse Sand		1	0.500	29.54	47.32
Medium/Fine Sand		4	0.063	51.69	99.00
Coarse Silt		5	0.031	1.00	100.00
Medium/Fine Silt		>5	<.031	0.00	100.00

excluded from analysis

% Debris	0.0		
Debris Type	0.001		

	mm	Phi	Cum. %	Fract. %
	4.0000	-2.0	0.0	0.0
	2.0000	-1.0	10.3	10.3

Grain Size Statistics (Folk & Ward)

	mm	phi	mm	Phi	Cum. %	Fract. %
			1.0000	0.0	17.8	7.5
			0.5000	1.0	47.3	29.5
Mean	0.533	0.91	0.2500	2.0	92.7	45.4
Median	0.454	1.14	0.1250	3.0	98.9	6.2
Sorting	0.506	0.98	0.0625	4.0	99.0	0.1
Skewness		-0.37	0.0313	5.0	100.0	1.0
Kurtosis		0.99	0.0078	7.0	100.0	0.0
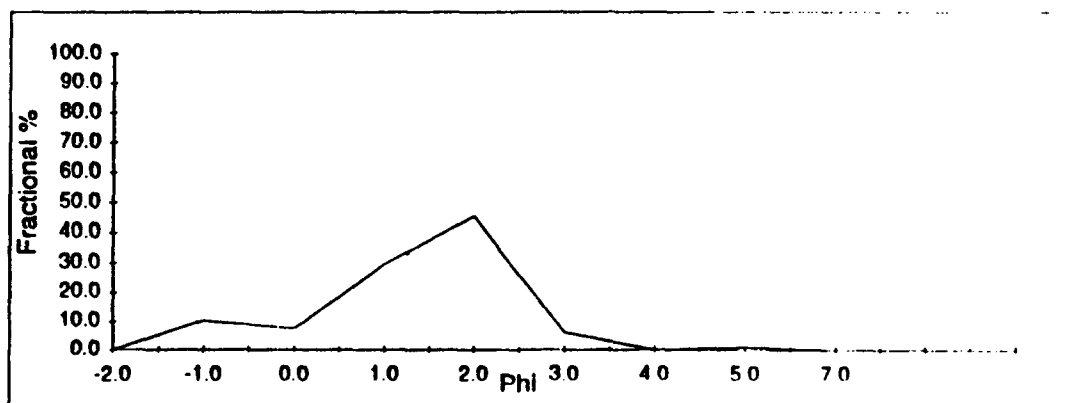
Project	CASP			Project #		93L
Sample I.D.	1-2Asilomar			Lab Number		0
Sample Date	9/29/93			Analysis Date	10\13\93	

	size ranges				
	phi	mm		Fract. %	Cum. %
Gravel	<0	>1.0		20.61	20.61
Coarse Sand	1	0.500		22.07	42.68
Medium/Fine Sand	4	0.063		56.45	99.13
Coarse Silt	5	0.031		0.87	100.00
Medium/Fine Silt	>5	<.031		0.00	100.00

excluded from analysis

$\quad$ *% Debris* $\quad$ 0.0

$\quad$ *Debris Type* $\quad$ 0.001

			mm	Phi	Cum. %	Fract. %
			4.0000	-2.0	0.0	0.0
			2.0000	-1.0	10.7	10.7
Grain Size Statistics (Folk & Ward)			1.0000	0.0	20.6	9.9
	mm	phi	0.5000	1.0	42.7	22.1
Mean	0.541	0.89	0.2500	2.0	98.2	55.5
Median	0.391	1.36	0.1250	3.0	98.9	0.8
Sorting	0.507	0.98	0.0625	4.0	99.1	0.2
Skewness		-0.65	0.0313	5.0	100.0	0.9
Kurtosis		0.88	0.0078	7.0	100.0	0.0

Project	CASP	Project #	93L
Sample I.D.	1-3Asilomar	Lab Number	0
Sample Date	9/29/93	Analysis Date	10\13\93

	size ranges			
	phi	mm	Fract %	Cum %
Gravel	<0	>1.0	12.68	12.68
Coarse Sand	1	0.500	25.82	38.50
Medium/Fine Sand	4	0.063	60.32	98.83
Coarse Silt	5	0.031	1.17	100.00
Medium/Fine Silt	>5	<.031	0.00	100.00

excluded from analysis
    % Debris 0.0
    Debris Type 0.001

	mm	Phi	Cum. %	Fract. %
	4.0000	-2.0	0.0	0.0
	2.0000	-1.0	6.9	6.9
Grain Size Statistics (Folk & Ward)	1.0000	0.0	12.7	5.8
	0.5000	1.0	38.5	25.8

	mm	phi	0.2500	2.0	90.7	52.2
Mean	0.443	1.17	0.1250	3.0	98.7	8.1
Median	0.364	1.46	0.0625	4.0	98.8	0.1
Sorting	0.535	0.90	0.0313	5.0	100.0	1.2
Skewness		-0.53	0.0078	7.0	100.0	0.0
Kurtosis		1.18				
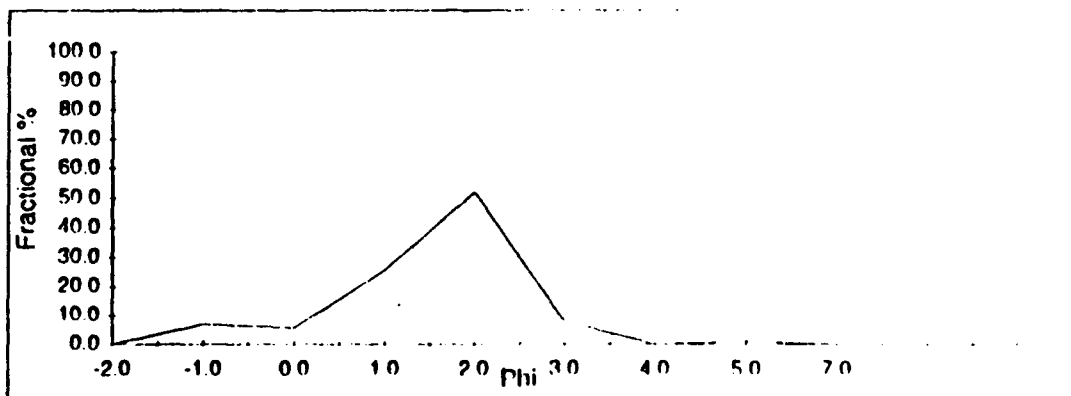
Project	CASP	Project #	93L
Sample I.D.	2-1NPS Bch	Lab Number	0
Sample Date	9/29/93	Analysis Date	10/13/93

	size ranges			
	phi	mm	Fract. %	Cum. %
Gravel	<0	>1.0	0.00	0.00
Coarse Sand	1	0.500	1.17	1.17
Medium/Fine Sand	4	0.063	97.51	98.68
Coarse Silt	5	0.031	1.32	100.00
Medium/Fine Silt	>5	<.031	0.00	100.00

excluded from analysis

% Debris 0.0
Debris Type 0.001

Grain Size Statistics (Folk & Ward)

	mm	phi
Mean	0.233	2.10
Median	0.230	2.12
Sorting	0.857	0.22
Skewness		-0.14
Kurtosis		1.27

mm	Phi	Cum. %	Fract. %
4.0000	-2.0	0.0	0.0
2.0000	-1.0	0.0	0.0
1.0000	0.0	0.0	0.0
0.5000	1.0	1.2	1.2
0.2500	2.0	25.8	24.6
0.1250	3.0	97.7	72.0
0.0625	4.0	98.7	0.9
0.0313	5.0	100.0	1.3
0.0078	7.0	100.0	0.0

Project	CASP		Project #	9 3L
Sample I.D.	2-2NPS Bch		Lab Number	0
Sample Date	9/29/93		Analysis Date	10\13\93

	size ranges			
	phi	mm	Fract. %	Cum. %
Gravel	<0	>1.0	0.08	0.08
Coarse Sand	1	0.500	1.31	1.41
Medium/Fine Sand	4	0.063	96.76	98.17
Coarse Silt	5	0.031	1.83	100.00
Medium/Fine Silt	>5	<.031	0.00	100.00

excluded from analysis

% Debris 0.0

Debris Type 0.001

			mm	Phi	Cum. %	Fract. %
			4.0000	-2.0	0.0	0.0
			2.0000	-1.0	0.0	0.0
Grain Size Statistics (Folk & Ward)			1.0000	0.0	0.1	0.1
	mm	phi	0.5000	1.0	1.4	1.3
Mean	0.244	2.03	0.2500	2.0	41.9	40.5
Median	0.243	2.04	0.1250	3.0	97.7	55.7
Sorting	0.847	0.24	0.0625	4.0	98.2	0.5
Skewness		-0.06	0.0313	5.0	100.0	1.8
Kurtosis		1.08	0.0078	7.0	100.0	0.0
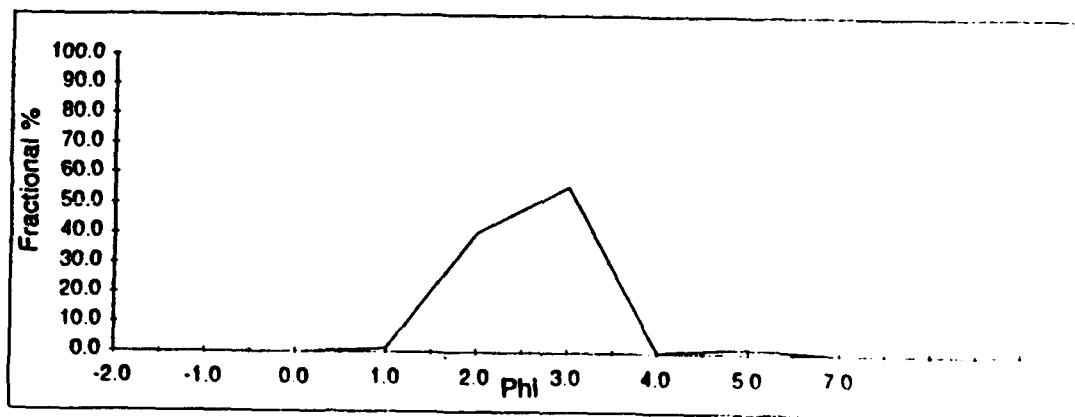
Project	CASP			Project #	9 ?.
Sample I.D.	2-3NPS Bch			Lab Number	0
Sample Date	9/29/93			Analysis Date	10\13\93

	size ranges			
	phi	mm	Fract. %	Cum. %
Gravel	<0	>1.0	0.01	0.01
Coarse Sand	1	0.500	1.26	1.27
Medium/Fine Sand	4	0.063	97.14	98.41
Coarse Silt	5	0.031	1.59	100.00
Medium/Fine Silt	>5	<.031	0.00	100.00

excluded from analysis

% Debris 0.0

Debris Type 0.001

Grain Size Statistics (Folk & Ward)

	mm	phi		mm	Phi	Cum. %	Fract. %
				4.0000	-2.0	0.0	0.0
				2.0000	-1.0	0.0	0.0
				1.0000	0.0	0.0	0.0
				0.5000	1.0	1.3	1.3
Mean	0.263	1.93		0.2500	2.0	70.0	68.7
Median	0.267	1.91		0.1250	3.0	97.6	27.7
Sorting	0.852	0.23		0.0625	4.0	98.4	0.8
Skewness		0.19		0.0313	5.0	100.0	1.6
Kurtosis		1.24		0.0078	7.0	100.0	0.0
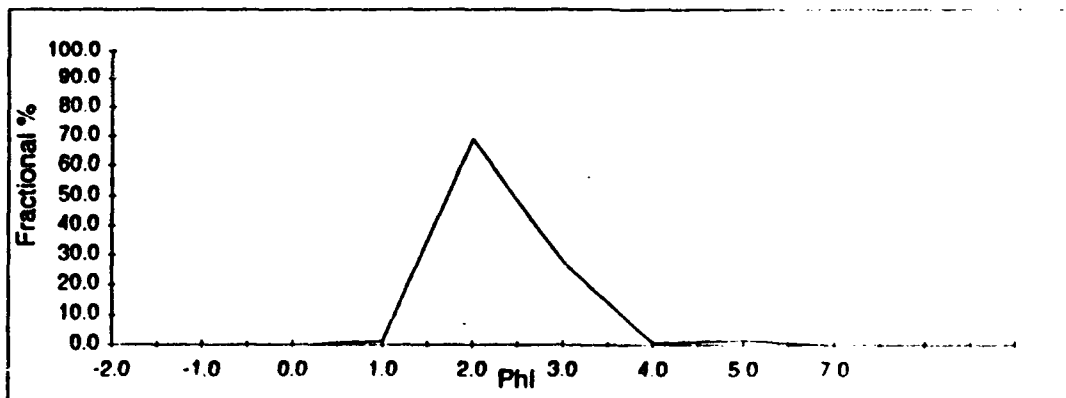
APPENDIX B

LIST OF SYMBOLS

a   equivalent particle radius

a_g geometric mean radius

a_0 transducer radius

c   sound speed in fluid

f_∞ backscatter form factor

k_c compression wave number

n(a)   particle size spectral density

p_s backscattered pressure amplitude

p_* on axis pressure amplitude at reference distance

r   perpendicular distance from transducer to detected volume

r_* reference distance

D   transducer directivity

J_1 cylindrical Bessel function of order 1

K_c digital counts of backscatter amplitude

M   mass concentration

S   overall system sensitivity

S_w	sensitivity calculated from wire targets
V	voltage output of receiver
α_0	attenuation coefficient in water
α_s	attenuation coefficient of scatterers
β	spreading angle of transducer
β_0	half power angle of the transducer
ϵ	Neumann factor
η_n	phase shift of nth wave
λ	acoustic wavelength
ρ_s	density of scatterer
σ_g	variance of lognormal distribution about geometric mean radius
τ	duration of transmitted pulse
ζ	combined attenuation by fluid and scatterer

LIST OF REFERENCES

Bosman, J.L., Van Der Velden, E.T.J.M., Hulsbergen, C.H., Sediment Concentration by Transverse Suction. *Coastal Engineering*, 11(4), November 1987.

Clay, C.S., and Medwin, H., *Acoustical Oceanography: Principles and Applications*, John Wiley, New York, 1977.

D & A Instrument Company, OBS-1 & 3 Instrument Manual, March 1991.

Faran, J.J.,Jr., Sound Scattering By Solid Cylinders and Spheres. *The Journal of the Acoustical Society of America*, 23(4), July 1951.

Hay, A.E., On the Remote Acoustic Detection of Suspended Sediment at Long Wavelengths. *The Journal of Geophysical Research*, 88(C12), September 1983.

Hay, A.E., Sound Scattering from a Particle-laden, Turbulent Jet. *The Journal of the Acoustical Society of America*, 90(4), October 1991.

Hay, A.E., and Mercer, D.G., On the Theory of Sound Scattering and Viscous Absorption in Aqueous Suspensions at Medium and Short Wavelengths. *The Journal of the Acoustical Society of America*, 78(5), November 1985.

Hay, A.E., and Sheng, J., Vertical Profiles of Suspended Sand Concentration and Size from Multifrequency Acoustic Backscatter. *The Journal of Geophysical Research*, Volume 97, No. C10, October 1992.

Sheng, J., and Hay, A.E. Spherical Wave Backscatter from Straight Cylinders: Thin-wire Standard Targets. *The Journal of the Acoustical Society of America*, 94(5), November 1993.

Stanton, T. P., The Coherent Acoustic Sediment Flux Probe (CASP), submitted to U. S. Army Corps of Engineers, Waterways Experiment Station, September 1993.

Varadan, V.K., Bringi, V.N., Varadan, V.V., and Ma, Y., Coherent Attenuation of Acoustic Waves by Pair-Correlated Random Distributions of Scatterers With Uniform and Gaussian Distributions., *The Journal of the Acoustical Society of America*, 73(6), June 1983.

INITIAL DISTRIBUTION LIST

1. Defense Technical Information Center 2
   Cameron Station
   Alexandria, VA 22304-6145

2. Library, Code 52 2
   Naval Postgraduate School
   Monterey, CA 93943-5002

3. Chairman, Department of Oceanography 1
   Code OC/Bo
   Naval Postgraduate School
   Monterey, CA 93943

4. Dr. Curtis A. Collins 1
   Code OC/Co
   Naval Postgraduate School
   Monterey, CA 93943

5. Timothy P. Stanton 2
   Code OC/St
   Naval Postgraduate School
   Monterey, CA 93943

6. Dr. Edward B. Thornton 2
   Code OC/Th
   Naval Postgraduate School
   Monterey, CA 93943

7. LT Weston J. Anderson 2
   PSC 473, BOX 68
   FPO AP 96349-2902

8. Dr. Tom White 1
   U.S. Army Engineers Waterways
   Experiment Station
   P.O. Box 631
   Vicksburg, MS 39180

9. Dr. Tom Kinder   1
    Coastal Sciences (Code 1121SS)
    800 North Quincy Street
    Arlington, VA 22217

10. Library   1
    Scripps Institution of Oceanography
    University of California, San Diego
    La Jolla, CA 92093